arXiv:1504.04493v1 [nucl-th] 17 Apr 2015

April 20, 2015

Unified treatment of sub-saturation stellar matter at zero and finite temperature

F. Gulminelli[1] and Ad. R. Raduta[2]
[1] *CNRS/ENSICAEN/LPC/Université de Caen Basse Normandy, UMR6534, F-14050 Caen cédex, France*
[2] *NIPNE, Bucharest-Magurele, POB-MG6, Romania*

The standard variational derivation of stellar matter structure in the Wigner-Seitz approximation is generalized to the finite temperature situation where a wide distribution of different nuclear species can coexist in the same density and proton fraction condition, possibly out of β-equilibrium. The same theoretical formalism is shown to describe on one side the single-nucleus approximation (SNA), currently used in most core collapse supernova simulations, and on the other side the nuclear statistical equilibrium (NSE) approach, routinely employed in r- and p-process explosive nucleosynthesis problems. In particular we show that in-medium effects have to be accounted for in NSE to have a theoretical consistency between the zero and finite temperature modeling. The bulk part of these in-medium effects is analytically calculated and shown to be different from a van der Waals excluded volume term. This unified formalism allows controlling quantitatively the deviations from the SNA in the different thermodynamic conditions, as well as having a NSE model which is reliable at any arbitrarily low value of the temperature, with potential applications for neutron star cooling and accretion problems. We present different illustrative results with several mass models and effective interactions, showing the importance of accounting for the nuclear species distribution even at temperatures lower than 1 MeV.

PACS numbers: 26.50.+x, 26.60.-c 21.65.Mn, 64.10.+h,

I. INTRODUCTION

Since the pioneering work of G.Baym and collaborators in the early seventies [1, 2], the theoretical formalism to variationally calculate the equation of state and composition of neutron star crusts with cluster degrees of freedom is well settled and has been exploited by many authors in the last decades [3–7]. Because of the crystalline structure of low density neutron star matter, the problem of neutron star structure at a given pressure is indeed reduced to the composition of a simple Wigner-Seitz cell, composed of a single nucleus immersed in a homogeneous gas of neutrons and electrons. The ground state of the system is then given by a set of coupled variational equations for the nucleus atomic and baryonic number (and shape, if the more exotic pasta phases are included), the volume of the cell, and the free neutron density [1, 2].

An alternative formulation within density functional theory was developed at the same time in another seminal paper for neutron star physics by J.Negele and D.Vautherin [8]. This entirely microscopic approach is in principle more appealing than a cluster model because it avoids the artificial distinction between clusters and free neutrons, and naturally accounts for the interface interaction between them. For this reason, and due to the great improvements of the predictive power of mean-field energy density functionals in the last decades [9–12], microscopic Hartree-Fock and Hartree-Fock-Bogoliubov methods have been widely employed for the computation of the neutron star equation of state [13–19]. As a consequence of this important collective theoretical effort, present uncertainties on the equation of state of neutron star matter at zero temperature are essentially limited to the still imperfect knowledge of the density dependence of the symmetry energy [20], which is itself better and better constrained thanks to the recent improvements in ab-initio neutron matter calculations [21–24].

Neutron stars being born hot, a natural extension of these works concern the consideration of finite temperature stellar matter, with applications ranging from neutron star cooling, accretion in binary systems and dynamics of supernova matter with associated nucleosynthesis problems. For these applications matter is typically out of β-equilibrium and therefore needs to be considered in a large interval of baryonic densities ρ_B and proton fractions y_p. Finite temperature mean-field calculations in the Wigner-Seitz cells have been largely employed [25–30]. However, because of the computational effort associated to these calculations, microscopic modeling of the finite temperature Wigner-Seitz cells is not adapted to the large scale calculations needed for supernova simulations, even if some large scale TDHF calculations start to be performed [31, 32, 34]. For this reason, hybrid models with cluster degrees of freedom are more appealing to address the finite temperature problem. The extension of the Baym et al. compressible liquid drop models to finite temperature was already proposed in the eighties [33] and allowed the elaboration of the famous Lattimer-Swesty [35] and Shen [36] supernova equation of state models, which are still widely used in present supernova simulations.

The problem of both microscopic and liquid-drop models is that they share the so-called Single-Nucleus-

Approximation (SNA), that is a unique configuration is assumed for each (T, ρ_B, y_p) thermodynamic condition, against the very principle of statistical mechanics which stipulates that finite temperature corresponds to a mixing of different microstates. In particular, in the LS and Shen EoS, besides free nucleons, only one kind of light cluster (α particles) and one kind of heavy cluster are assumed to exist. The idea is to account in an average way for the properties of the statistical cluster distribution. The SNA may not affect very strongly thermodynamical properties of matter in the temperature and density domains of interest [37], but it has important consequences for dynamical processes dependent on reaction rates of specific nuclei [38, 39] and for the gas-liquid phase transition. Therefore, more modern approaches rely on an extended nuclear statistical equilibrium (NSE) concept, where the distribution of clusters over, in principle, all mass numbers is taken into account and obtained self-consistently under conditions of statistical equilibrium [40–43]. Originally, the NSE was introduced to describe the reaction network taking place at the end of the evolution of massive stars in red supergiants [40]. Being very diluted, nuclei interact weakly and are almost not modified by the surrounding medium. These conditions naturally lead to the Saha equations. The NSE in the dense and hot matter in the core of supernovae was first applied in the EoS of Hillebrandt and Wolff [44].

In recent NSE implementations [45–49], the interactions between a cluster and the surrounding gas is treated in the so-called excluded-volume approach. The clusters and the gas of light particles do not overlap in space and the clusters binding energy is kept as in the free limit. It is known, however, from virial expansion at low density and quantal approaches [50–53], that the cluster properties are modified by the coexistence with a gas. Moreover, the excluded volume treatment of cluster-nucleon interaction is not compatible with microscopic calculations in the Wigner-Seitz cell, where cluster properties are naturally modified by the surrounding gas by the density dependence of the self-consistent mean-field and the Pauli-blocking effect of occupied single-particle states. The conceptual difference between the classical excluded-volume picture and the quantal picture emerging from microscopic calculations was discussed in ref. [54]. It leads to two different definitions of clusters in dense media, namely configuration-space and energy-space clusters, with different particle number and energy functionals. Including one or the other of the two definitions in a finite temperature NSE partition sum will naturally produce differences in the observables, even if the total free energy of the Wigner Seitz cell entering in the SNA approaches [35, 36] does not depend by construction on the cluster definition [54]. As a consequence, it is not clear if the NSE models have the correct limit towards $T = 0$, where the SNA approximation becomes exact. Recent comparisons [55] between different models indicate that huge differences exist among the different models even at very low temperature, suggesting that the zero temperature limit is not fully under control. Such an uncontrolled model dependence might be an important hindrance to pin down the EoS dependence of supernova dynamics [56, 57].

In this paper we develop an analytical unified theoretical formalism to describe on one side the single-nucleus approximation (SNA), and on the other side the nuclear statistical equilibrium (NSE) approach. To this aim, we map the energetics and composition of a microscopic Wigner-Seitz cell into a model of the same cell with cluster degrees of freedom. If a density and isospin dependent modification of the cluster surface energy is included, this cluster model can thus exactly span the full spectroscopy (ground state and excited states) of the extended Thomas-Fermi (ETF) approximation [29] with the only uncertainty given by the employed energy density functional.

A variational minimization of the total free energy of the Wigner-Seitz cell with respect to the cell composition leads to the standard SNA equilibrium approach, at zero as well as finite temperature. A complete finite temperature treatment is obtained by calculating the partition sum of a system of independent cells, leading to a statistical distribution of cells with different compositions. NSE equations naturally emerge from this treatment, but energy-space clusters are demonstrated to be the correct degrees of freedom in order to get a consistent treatment towards the zero temperature limit. We also show that a cut-off in the cluster density of states has to be applied in order to avoid double counting of scattering states.

The first part of the paper is devoted to zero temperature. Section II A defines the degrees of freedom and associated energy functionals used in this work. Section II B gives the variational equations to be solved at zero temperature to get the ground state of stellar matter. The non-standard case where β equilibrium is not imposed is also considered. This case is not physically realistic, but gives the reference zero temperature limit of supernova matter, thus guaranteeing the consistency of the finite temperature formalism. To maximize the predictive power of the formalism, an experimental nuclear mass table is used in section II C to predict the composition of the neutron star crust, and results are compared to the rich literature available on this subject. The equation of state is briefly addressed in Section II D, and to conclude the zero temperature discussion, the issue of phase transitions is analyzed in section II E. We demonstrate on very general arguments that the constraint of charge neutrality quenches the first order nuclear matter liquid-gas phase transition. A residual very narrow transition region exists at densities of the order of $\rho_0/5 - \rho_0/3$, depending on the interaction, which physically corresponds to the emergence of pasta phases.

In the second part of the paper, we switch to finite temperature. Section III A gives the derivation of the coupled variational equations in the SNA approximation, as well as some applications in β-equilibrium. Sections III B, III C build the partition sum of the model in the canonical and in the grandcanonical ensemble, leading to the derivation of the generalized NSE equations, which are compared to the SNA approximation in section III D. Finally section IV

gives a summary and conclusions.

II. ZERO TEMPERATURE STELLAR MATTER

A. Energy in the Wigner-Seitz cell

Let us define a zero temperature thermodynamic condition for compact star matter as a given value for the baryon density and proton fraction, (ρ_B, y_p). Since by definition there is no interaction among Wigner-Seitz cells, the energy density of the system is given by:

$$\epsilon_{NS}(\rho_B, y_p) = \lim_{N\to\infty} \frac{\sum_{i=1}^{N} E_{WS}(i)}{\sum_{i=1}^{N} V_{WS}(i)}, \tag{II.1}$$

where $E^{WS}(i)$ is the energy of the $i-th$ WS cell. Each cell consists of N_{WS} neutrons and Z_{WS} protons in a volume V_{WS}. We make the standard simplifying approximation that the cell consists of a single cluster with the possible addition of an homogeneous nuclear gas. This approximation is inspired by the numerical results of microscopic calculations [13–19]. However, this approximation is not fully realistic since it is also well known that at finite temperature light clusters can coexist with the single heavy nucleus[58, 59]. For this reason in the Lattimer-Swesty equation of state α particles are added to the nucleon gas inside the Wigner-Seitz cell[35], but interactions between the α's and the cluster (or the gas) are neglected in that model. This coexistence effect of heavy and light clusters will be automatically accounted by our formalism, because in the NSE model section III C the equilibrium configuration will consist in a mixture of different WS cells containing clusters of all species. However, two-body Coulomb and possibly nuclear effects due to multiple clusters inside a same cell are out of the scope of the present treatment, and each (light or heavy) cluster will be associated to its proper WS cell.

As we shall explicitly work out, for a given set (A_{WS}, I_{WS}, V_{WS}) $(A_{WS} = N_{WS} + Z_{WS}, I_{WS} = N_{WS} - Z_{WS})$ equilibrium imposes a unique mass and composition of the cluster and of the gas. Five variables define this mass and composition, namely: the cell volume V_{WS}, the gas density and composition $\rho_g = \rho_{ng} + \rho_{pg}$, $y_g = \rho_{ng} - \rho_{pg}$, where ρ_{ng} (ρ_{pg}) is the density of neutrons (protons) in the gas, and the neutron N and proton Z numbers associated to the cluster. The total energy in the Wigner-Seitz cell is written as $E^{tot}_{WS} = Z_{WS} m_p c^2 + N_{WS} m_n c^2 + E_{WS}$ with:

$$E_{WS} = E^{vac}(A, \delta) + V_{WS}\left(\epsilon_{HM}(\rho_g, y_g) + \epsilon_{el}(\rho_e)\right) + \delta E. \tag{II.2}$$

Here, ϵ_{HM} is the energy density of uniform asymmetric nuclear matter, ϵ_{el} is the energy density of a uniform electron gas at the density $\rho_e = y_p \rho_B$ imposed by charge neutrality, E^{vac} is the cluster energy in the vacuum, and δE is the in-medium modification due to the interaction between the cluster and the gas. An important part of the in-medium correction is given by the Coulomb screening by the electron gas, and by the Pauli-blocking effect of high energy cluster single particle states due to the gas [52]. This latter effect can be approximately accounted for by subtracting from the local energy density the contribution of the unbound gas states. We call "e-cluster" [54] the left-over bound part of the cluster. Equation (II.2) is then conveniently written as:

$$E_{WS} = E^{e}(A, \delta, \rho_g, y_g)(A, \delta) + V_{WS}\left(\epsilon_{HM}(\rho_g, y_g) + \epsilon_{el}(\rho_e)\right). \tag{II.3}$$

In this expression, E^e is the in-medium modified cluster energy in the e-cluster representation:

$$E^{e}(A, \delta, \rho_g, \delta_g, \rho_p) = E^{vac}(A, \delta) - \epsilon_{HM}(\rho_g, \delta_g)\frac{A}{\rho_0(\delta)} + \delta E_{surf} + \delta E_{Coulomb}, \tag{II.4}$$

where δ is the bulk isospin asymmetry, and the residual in-medium energy shift δE_{surf} can be shown to behave as a surface term [54, 60].

It is interesting to observe that eq.(II.3) can be equivalently written as:

$$E_{WS} = (V_{WS} - V_0)\,\epsilon_{HM}(\rho_g, y_g) + V_{WS}\epsilon_{el} + E^{vac}(A, \delta)(A, \delta) + \delta E_{surf} + \delta E_{Coulomb}, \tag{II.5}$$

where $V_0 = A/\rho_0(\delta)$ is the equivalent cluster volume corresponding to δ isospin asymmetry and $\rho_0(\delta)$ is the saturation density of nuclear matter at the asymmetry δ. In this representation, that we call "r-cluster" representation [54], the in-medium effects only affect the surface properties of the cluster. The in-medium bulk term apparent in eq.(II.4) is here interpreted as an excluded volume. At variance with the classical Van der Waals model, this "excluded volume" is not a simple limitation of the r-space integral of the partition sum, but it directly affects the energetics of the Wigner-Seitz cell.

It is also useful to introduce the bound part of the cluster (or equivalently: size of the e-cluster) defined as:

$$A_e = A\left(1-\frac{\rho_g}{\rho_0(\delta)}\right), \tag{II.6}$$

$$Z_e = Z\left(1-\frac{\rho_{pg}}{\rho_{0p}(\delta)}\right). \tag{II.7}$$

For simplicity, in the following variational derivation of the equilibrium equations we shall initially assume $\delta = 1-2Z/A$ which implies neglecting skin and Coulomb effects. However, we will include this effect in Section III C.

The different contributions to the energy are defined as follows. The presence of electrons in the cell modifies the cluster energy with respect to its vacuum value as

$$E^0(A,\delta,\rho_e) = E^{nuc}(A,Z,\rho_e) + V_{WS}\epsilon_{el}(\rho_e) = E^{vac} + \delta E_{coul} + V_{WS}\epsilon_{el}, \tag{II.8}$$

where the Coulomb energy is modified by the electron screening

$$\delta E_{coul} = a_c f_{WS}(\delta,\rho_e)A^{5/3}\frac{(1-\delta)^2}{4}, \tag{II.9}$$

with the Coulomb screening function in the Wigner-Seitz approximation:

$$f_{WS}(\delta,\rho_e) = \frac{3}{2}\left(\frac{2\rho_e}{(1-\delta)\rho_0}\right)^{1/3} - \frac{1}{2}\left(\frac{2\rho_e}{(1-\delta)\rho_0}\right), \tag{II.10}$$

and the electron energy density containing the rest mass contribution is given by [1]

$$\epsilon_{el} = \frac{m_e^4c^5}{8\pi^2\hbar^3}\left[\left(2t^2+1\right)t\left(t^2+1\right)^{1/2} - \ln\left(t+\left(t^2+1\right)^{1/2}\right)\right], \tag{II.11}$$

where $t = \hbar(3\pi^2\rho_e)^{1/3}/m_ec$. The total electron chemical potential (including rest mass contribution) is defined as a function of the total proton density $\rho_p = y_p\rho_B$ by

$$\mu_{el}^{tot} = d\epsilon_{el}/d\rho_e(\rho_e=\rho_p) = \frac{m_e^3c^4}{8\pi^{4/3}\hbar^2}\frac{1}{3^{2/3}}\rho_e^{-2/3}\left[(t^2+1)^{1/2}(1+6t^2) + \frac{t^2(2t^2+1)}{(t^2+1)^{1/2}} - \frac{1}{(1+t^2)^{1/2}}\right]. \tag{II.12}$$

Unless otherwise explicitly mentioned, we will use for the energy functional of the cluster in vacuum, $E_{vac}(A,Z)$, the table of experimental masses of Audi *et al.* [61], publicly available in electronic format. When these latter are not known, which is typically the case close and above the drip-lines, we will use a liquid-drop parameterization [62] with coefficients fitted out of HF calculations using the same Skyrme effective interaction which is employed for the homogeneous gas. This parameterization, hereafter called Skyrme-LDM model, reads:

$$\frac{E_{LDM}^{vac}}{A} = a_v - a_sA^{-1/3} - a_a(A)\delta^2 - a_cA^{2/3}\frac{(1-\delta)^2}{4}, \tag{II.13}$$

with the asymmetry energy coefficient:

$$a_a(A) = \frac{a_v^a}{1+\frac{a_v^a}{a_s^aA^{1/3}}} \tag{II.14}$$

For the numerical applications concerning the NSE model in section III C, this parameterization will be supplemented in the case of even mass nuclei with a simple phenomenological pairing term, $\Delta(A) = \pm 12/\sqrt{A}$ where +(-) corresponds to even-even (odd-odd) nuclei. The in-medium surface correction $\delta E_{surf}(A,\delta,\rho_g,\delta_g)$ due to the interaction with the surrounding gas can in principle be accounted for by a density dependent modification of the surface and symmetry-surface coefficients. A determination of these coefficients within the extended Thomas-Fermi model [60] will be published elsewhere [63]. For the numerical applications of this paper, we will ignore this correction, and consider that the main in-medium effect is given by the bulk nuclear and Coulomb binding energy shift.

Below saturation, the Coulomb screening effect of the electrons is never total. This implies that only a finite number $N_{species}$ of nuclear species (A,Z) can exist at zero temperature, and consequently a finite number of WS cells $N_{WS}(\rho_B,y_p) = N_{species}$. Eq. (II.1) then becomes:

$$\epsilon_{NS}(\rho_B,y_p) = \sum_{k=1}^{N_{WS}(\rho_B,y_p)}\frac{E_{WS}(k)}{V_{WS}(k)}p(k) \;\;;\;\; p(k) = \lim_{N_k,V\to\infty}\frac{N_kV_{WS}(k)}{V}, \tag{II.15}$$

where V is the total volume. The Single Nucleus Approximation (SNA) [35] consists in considering $N_{WS}(\rho_B, y_p) = 1, p(1) = 1$. This approximation is exact at zero temperature in the absence of phase transitions, and in principle should fail at finite temperature, even in the absence of phase transitions. In the following we explore if phase transitions are there or not, and the degree of violation of SNA at finite temperature.

B. Zero temperature solution in the SNA

The variational formalism to obtain the composition of stellar matter at zero temperature has been proposed long ago [1, 2] and regularly employed since then, using more sophisticated models for the nuclear energetics [64–67]. We will follow the very same strategy, but at variance with the seminal papers [1, 2] , we will determine the optimal configuration for each given (ρ_B, y_p) point without implementing β-equilibrium in the variational constraints. This choice will allow us keeping the same formalism for neutron star crust and the finite temperature supernova matter, which is not in β-equilibrium. Concerning the specific application to the NS crust, we will determine in a second step the $y_p(\rho_B)$ relation imposed by β-equilibrium.

The variables to be variationally found are $(A, \delta, \rho_{ng}, \rho_{pg}, V_{WS})$. The two constraints, which will lead to the introduction of two chemical potentials, can be written as:

$$\rho_g = \frac{1}{V_{WS}} \left(A_{WS} - A_e\right), \tag{II.16}$$

$$y_g = \frac{1}{V_{WS}} \left(I_{WS} - I_e\right). \tag{II.17}$$

Using the relation (II.6),(II.7) between r-clusters and e-clusters we can write the auxiliary function to be minimized:

$$\begin{aligned} \mathcal{D}(A, \delta, \rho_g, y_g, V_{WS}) &= \epsilon_{HM}(\rho_g, y_g) + E^e(A, \delta, \rho_g, y_g)/V_{WS} \\ &- \alpha\rho_g \left(\rho_0 - A/V_{WS}\right) + \alpha\rho_0 \left(\rho_B - A/V_{WS}\right) \\ &- \beta y_g \left(\rho_0 - A/V_{WS}\right) + \beta\rho_0 \left(\rho_B(1 - 2y_p) - A\delta/V_{WS}\right). \end{aligned} \tag{II.18}$$

An additional complication comes from the fact that at zero temperature the gas can only be a pure gas.

Indeed within the neutron and proton drip-lines a pure nucleus solution is by definition more bound than a solution where one particle would be in the gas. The drip-lines are defined by the lowest N (Z) solution of the equations:

$$E^{nuc}(N+1, Z, \rho_e) - E^{nuc}(N, Z, \rho_e) \geq 0 \; ; \; E^{nuc}(N, Z+1, \rho_e) - E^{nuc}(N, Z, \rho_e) \geq 0. \tag{II.19}$$

Notice that because of the electron screening the drip-lines in the neutron star crust are displaced with respect to nuclei in the vacuum, and in particular the fission instability line does not exist. However eqs.(II.19) admit a solution for any N, Z, meaning that when the equilibrium solution is below that line the nucleus will be in equilibrium with the vacuum. Above the neutron (proton) drip-line, we will have an equilibrium with a neutron (proton) vacuum gas. This $T = 0$ anomaly is very well known in nuclear matter. An equilibrium with the vacuum does not impose an equality between two chemical potentials, because the vacuum has $\mu = 0$. If a system with A particles and energy $E(A)$ is in equilibrium with the vacuum, its chemical potential is defined by a one-sided Maxwell construction between $E(A = 0) = 0$ and $E(A)$ with slope $E(A)/A$. The chemical potential of this particular equilibrium is given by:

$$\mu \equiv \frac{dE}{dA} = \frac{E}{A}, \tag{II.20}$$

which implies $d(E/A)/dA = 0$, that is the equilibrium solution minimizes the energy per particle (and not the total energy, as it is the case in a finite well defined volume V).

Coming back to the minimization of the auxiliary function eq.(II.18), the minimization with respect to the gas densities gives:

$$\alpha + \beta = \frac{\mu_n}{\rho_0} = \frac{\mu_g}{\rho_0} \quad iff \quad \rho_{gn} > 0 \; ; \; \alpha - \beta = \frac{\mu_p}{\rho_0} = \frac{\mu_g}{\rho_0} \quad iff \quad \rho_{gp} > 0. \tag{II.21}$$

If one of the two densities is zero, that is below the corresponding drip-line, we lose one equation but also one unknown, and one can use one of the conservation equations to determine the missing variables. The result is a system of four

coupled equations:

$$\rho_{Bp(n)} = \frac{A(1\mp\delta)}{2V_{WS}}, \tag{II.22}$$

$$\rho_{Bn(p)} = \rho_g\left(1-\frac{A}{\rho_0 V_{WS}}\right)+\frac{A(1\pm\delta)}{2V_{WS}}, \tag{II.23}$$

$$\frac{\partial(E^{nuc}/A)}{\partial A}|_\delta = 0, \tag{II.24}$$

$$\frac{1}{A}\frac{\partial E^e}{\partial\delta}|_A \pm \frac{1}{1\mp\delta}\frac{\partial E^e}{\partial A}|_\delta = \pm\mu_g\frac{1}{1\mp\delta}\left(1-\frac{\rho_g}{\rho_0}\right)+\mu_g\frac{\rho_g\rho_0'}{\rho_0^2}. \tag{II.25}$$

The upper (lower) sign refers to a neutron (proton) gas, $\rho_{Bp(n)}$ indicates the proton (neutron) baryon density for a neutron (proton) gas, $\rho_g=\rho_{n(p)g}$, $\mu_g=\partial\epsilon_{HM}/\partial\rho_{n(p)g}$. The two last equations suppose that E^{nuc} is a differentiable function of A and δ, which is obviously not the case if we take experimental masses. In this case the derivatives have to be interpreted as finite differences. We can see that the Coulomb screening effect of the electrons enters in the equilibrium equations, while the kinetic energy of the electrons does not play any role in the equilibrium sharing. This is the reason why this term is usually disregarded out of β equilibrium. However we will see that it will play a role at finite temperature, determining the possible existence of phase transitions.

Different observations are in order.

First, from eq.(II.24) we can see that, both below and above the drip, the minimization conditions correspond to the minimization of the energy per nucleon with respect to the nucleus size, at the isospin value imposed by the constraint and the chemical equilibrium with the gas eq.(II.25). Concerning eq.(II.25), the coupling of the isoscalar to the isovector sector is trivially due to the fact that we are using $(A,\delta=AI)$ as isoscalar and isovector variables instead than (A,I) which would be the more natural choice if we did not have $\rho_0=\rho_0(\delta)$. With this choice of variables, if we consider the textbook example of two ideal gases composed of two different species of molecules 1, 2, $E=E_1(A_1,I_1)+E_2(A_2,I_2)$ fulfilling the conservation equations

$$A=A_1+A_2\ ;\ I=I_1+I_2, \tag{II.26}$$

using the same Lagrange multiplier method as before and defining $\mu,\tilde{\mu}$ as the chemical potentials of component 2, we find the classical equality of chemical potentials if we work with the variables (A,I):

$$\frac{\partial E_1}{\partial A_1}|_{I_1}=\frac{\partial E_2}{\partial A_2}|_{I_2}=\mu\ ;\ \frac{\partial E_1}{\partial I_1}|_{A_1}=\frac{\partial E_2}{\partial I_2}|_{A_2}=\tilde{\mu}, \tag{II.27}$$

while we have a coupling to the isovector sector for the mass sharing equation if we work with (A,δ):

$$\frac{\partial E_1}{\partial A_1}|_{\delta_1}=\mu+\delta_1\tilde{\mu}\ ;\ \frac{\partial E_1}{\partial \delta_1}|_{A_1}=A_1\tilde{\mu}. \tag{II.28}$$

This is a very natural result, because with this choice of variables the two constraints are not independent any more, that is the constraint associated to the β multiplier contains the variable A_1.

Second, the factor $(1-\rho_g/\rho_0)$ introduces a coupling between the two subsystems cluster and gas, that is an interaction. This comes from that fact that our two systems are in fact coupled: the energy of the cluster depends on the composition of the gas as it can be seen from eq.(II.4). This coupling is due to the fact that a part of the high density part of the Wigner-Seitz cell is constituted by the gas. From eq.(II.5) , we can see that this is an effect of the excluded volume which enters the mass conservation constraint. In the e-cluster language (see eq.(II.3)), we can equivalently say that it is an effect of the self-energy shift of the e-cluster inside the gas. This shows that the excluded volume indeed acts as an interaction. This effect goes in the direction of reducing the effective chemical potential with respect to the non-interaction case, that is reducing the cluster size. If we account for the cluster compressibility, that is the δ dependence of ρ_0, an extra effective coupling emerges (last term in the r.h.s. of eq.(II.25)).

In the case of moderate asymmetries below the neutron drip, the set of coupled equations eqs.(II.22),(II.23),(II.24),(II.25) reduces to the single equation eq.(II.24) giving the most stable isotope for a given asymmetry. If we assume a functional form as eq.(II.13) for the cluster energy functional, this equation admits an analytical solution:

$$a_s-\frac{a_a^2(A)}{a_s^a}\delta^2=\frac{a_c}{2}(1-f_{WS}(\delta,\rho_e))\,(1-\delta)^2\,A. \tag{II.29}$$

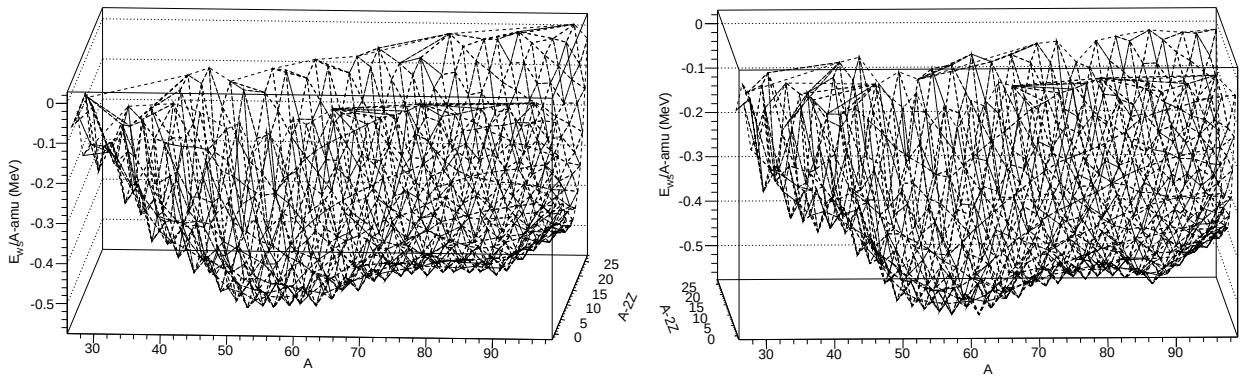

FIG. II.1: (Color online). Surface of the total energy per baryon at $\rho_B = 10^7$ fm^3 and different values of proton fractions. The cluster energy is calculated according to FRDM [69] (left) and using the experimental database [61] (right).

The solution is particularly simple in the case of symmetric nuclei $\delta = 0$:

$$A^{eq}(\delta = 0) = \frac{2a_s}{a_c(1 - f_{WS})}. \tag{II.30}$$

In the vacuum $\rho_e = 0, f_{WS} = 0$ and we get a nucleus around $A \approx 55$, $A^{eq} = 2a_s/a_c$, while at saturation density $\rho_e = \rho_{0p} = \rho_0/2$ $A^{eq} \to \infty$, showing that we do obtain the homogeneous matter limit at saturation.

C. The structure of the neutron star crust

The different solutions of eqs.(II.22)-(II.25) lead to a unique composition $(A, \delta, \rho_g, V_{WS})$ for each couple of external constraints (ρ_B, y_p). Let us consider the energy density, $\epsilon_{WS}(\rho_B, y_p) = E^{tot}_{WS}/V_{WS}$. It contains a baryonic and a leptonic part, $\epsilon_{WS}(\rho_B, y_p) = (\rho_p m_p + \rho_n m_n)c^2 + \epsilon_B(\rho_B, y_p) + \epsilon_{el}(\rho_e = \rho_p)$. In the long-lived neutron star, the proton and neutron densities do not correspond to separate conservation laws because weak processes transforming protons into neutrons are in complete equilibrium. The structure of the neutron star crust is then obtained by choosing, among all the different Z_{WS} values corresponding to different values of the proton fraction y_p, the one leading to an absolute minimum of the energy density. This minimization condition reads:

$$\epsilon^{\beta eq}_{WS}(\rho_B) = \min_{y_p} \left(\epsilon_{WS}(\rho_B, y_p)\right). \tag{II.31}$$

In the inner crust above the neutron drip the densities are continuous variables and the energy density is a differentiable function. Using the variable change $2\rho_n = \rho_B + \rho_3$, $2\rho_p = \rho_B - \rho_3$, the minimization then trivially gives the usual chemical β-equilibrium condition

$$\frac{\partial \epsilon_{WS}}{\partial \rho_n} - \frac{\partial \epsilon_{WS}}{\partial \rho_p} = m_n c^2 + \frac{\partial \epsilon_B}{\partial \rho_n} - m_p c^2 - \frac{\partial \epsilon_B}{\partial \rho_p} - \frac{\partial \epsilon_{el}}{\partial \rho_p} = \mu^{tot}_n - \mu^{tot}_p - \mu^{tot}_e = 0, \tag{II.32}$$

where $\mu^{tot}_i = m_i c^2 + \partial\epsilon/\partial\rho_i$ is the chemical potential including the rest mass contribution.

Below the drip-line (outer crust), the minimization condition (II.31) reduces to:

$$\epsilon^{\beta eq}_{WS}(\rho_B) = \min_Z \left(\frac{E^{nuc}(A, Z, \rho_e)}{V_{WS}} + \rho_n m_n c^2 + \rho_p m_p c^2 + \epsilon_e \right). \tag{II.33}$$

The value of Z leading to the minimal energy $Z = Z_{\beta eq}(A)$ corresponds to the equilibrium nucleus. This is still a β-equilibrium condition, but it has to be interpreted as the ensemble of two inequalities:

$$\mu^{tot}_n(N-1, Z+1) - \mu^{tot}_p(N, Z) - \mu^{tot}_e(Z) \ < \ 0, \tag{II.34}$$

$$\mu^{tot}_n(N, Z) - \mu^{tot}_p(N+1, Z-1) - \mu^{tot}_e(Z-1) \ > \ 0. \tag{II.35}$$

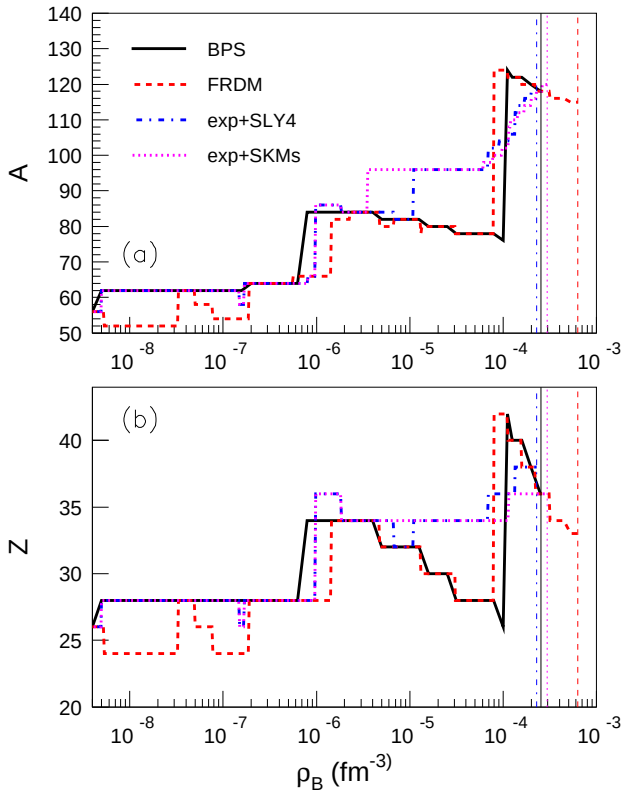

FIG. II.2: (Color online). Outer crust composition at T = 0: Baryonic (top panel) and atomic (lower panel) numbers of the β-equilibrium nucleus as a function of the baryonic density. BPS corresponds to predictions by BPS[1]; FRDM and exp+SLY4(SKMs) stand for present model predictions when nuclear masses are calculated according to Finite-Range Droplet Model of Ref.[69] and, respectively, atomic mass data of Ref.[61] + LDM-SLY4 (SKMs) model of Ref.[62]. The vertical lines mark the drip-line in the stellar medium.

In this set of inequalities, $\mu_n^{tot}(N,Z)d\rho_n = \epsilon_B(N+1,Z) - \epsilon_B(N,Z)$ with $\epsilon_B(N,Z) = (E^{nuc}(N,Z) + Nm_nc^2 + Zm_pc^2)/V_{WS}(N,Z)$. An equivalent relation holds for μ_p^{tot}.

Most of the published studies on the composition of the neutron star crust employ empirical mass formulas [1, 2] or microscopic functionals from self-consistent HFB calculations [64–68] to describe the cluster energy functional E^{vac}. The advantage of such an approach is that the derivatives in eq.(II.24),(II.25) can be analytically performed. A functional approach is unavoidable in the inner crust, because no experimental measurement exists above the drip-line. Conversely, in the outer crust the predictive power of the approach entirely depends on the quality of the mass formula to describe experimental data. Now, it comes out that the energy surface in the presence of the electron gas has a huge number of quasi-degenerate minima.

This is shown for an arbitrary chosen density within the outer crust $\rho_B = 10^{-7}$ fm^{-3} in Figure II.1. This figure shows the energy surface of the equilibrium Wigner-Seitz cells corresponding to different y_p values obtained using the FRDM parameterization by Moller and Nix from ref. [69] as well as the measured nuclear masses from ref. [61]. We can see that, though the FRDM predictions are very close to the measured mass, the obvious tiny differences can affect the determination of the absolute minimum. This means that even modern highly predictive mass formulas describing nuclear masses within 0.5 MeV or even less can lead to inexact results when applied to the outer crust.

The importance of this model dependence is shown in Figure II.2 and table II C.

Let us first discuss the outer crust, on the left of the vertical lines in Fig.II.2. We can see that the use of an experimental mass table leads to sizable differences even with sophisticated mass formulas like the FRDM model [69].

In the inner depths of the outer crust, the equilibrium nucleus is so neutron rich that no mass measurement exists. Then the crust composition depends on the theoretical cluster functional employed, and more specifically on its properties in the isovector channel, which are still largely unknown. As it is well known, this induces a strong model dependence on the composition. As shown in Table II C, model independent results can be obtained up to about $\rho_B = 10^{-5}$ fm^{-3}. At that density the solution of the variational equations solved using the SLY4 functional when

TABLE I: Composition of the outer layer of the outer crust of a cold neutron star as a function of baryonic density. FRDM and exp+SLY4 stand for model predictions when nuclear masses are calculated according to Finite-Range Droplet Model of Ref.[69] and, respectively, atomic mass data of Ref.[61] + SLY4 model of Ref.[62]. The atomic and mass numbers in italics for the set exp+SLY4 correspond to nuclides for which experimental mass evaluations (or extrapolations) do not exist.

FRDM			exp+SLY4		
ρ_B (fm^{-3})	A	Z	ρ_B (fm^{-3})	A	Z
1.000e-10	56	26	1.000e-10	56	26
5.370e-9	52	24	5.012e-9	62	28
3.311e-8	62	28	1.513e-7	58	26
5.012e-8	58	26	1.698e-7	64	28
7.762e-8	54	24	8.128e-7	66	28
1.905e-7	64	28	9.772e-7	86	36
5.623e-7	66	28	1.862e-6	84	34
1.445e-6	82	34	6.761e-6	82	32
2.291e-6	84	34	1.096e-5	*96*	*34*
4.786e-6	80	32	6.918e-5	*102*	*36*
6.761e-6	82	32	9.120e-5	*104*	*36*
1.349e-5	80	30	1.148e-4	*106*	*36*
3.090e-5	78	28			
7.943e-5	124	42			
1.122e-04	122	40			
1.585e-04	120	38			

experimental masses are not available, produces as preferred isotope ^{96}Se ($A = 96, Z = 34$). Now, the smallest Z for which an experimental mass exists for A=96 is Z=35 showing that this solution is due to a mismatch between the prediction of the SLY4 functional and the experimental data. The results in italic in table II C are therefore not reliable. The observed deviation in Fig.II.2 between exp+SLY4 and exp+SKMs is similarly due to the fact that the mismatch is bigger with the less performant SKMs functional. The full model independence of the outer crust composition is confirmed by the fact that our results for the outer crust are in agreement with refs.[65, 66]. This essentially shows that our variational equations are correctly solved. In ref.[65] the model-independent region is slightly larger than in our work, because they have used the FRDM model to complement the experimental information when unavailable, and this latter, as we have already stressed, has a smaller mismatch with experimental data.

Whatever the predictive power of the mass model, a model dependence is unavoidable in the inner crust, where the equation of state of the pure neutron gas directly enters in the minimization equations [68]. To illustrate this point, we show in Fig.II.3 the total composition of the neutron star crust obtained with different models. Whatever the equation of state, the predictions of eqs.(II.22)-(II.25) show that, in the inner crust, the mass and charge of the unique nucleus of the WS cell continously increase with baryonic density and then suddenly fall to zero. The abrupt cluster disappearence occurs because, depending of the employed interaction, at a density of the order of $\rho_0/5 - \rho_0/3$ homogeneous matter becomes energetically more favorable than clusterized matter. This is shown for a representative effective interaction in the right panel of Fig. II.6 where the baryonic density dependence of the constrained energy densities of β-equilibrated clusterized and homogeneous matter at T=0 are compared. Because of this behavior, the crust-core transition was typically considered as (weakly) first order in the literature [2]. It is however nowadays well established that at the density of nuclei dissolution non-spherical pasta are energetically favored, making the transition continuous. We will come back to this point in section II E.

The effect of the nuclear matter equation of state in the prediction of the composition of the inner crust has been studied in detail in the recent years [66, 68]. It leads to the difference in Fig.II.3 between the dotted and dash-dotted line, which represent two characteristic equations of state. A more extensive study of the different Skyrme interactions is beyond the scope of this paper, however some extra results on this subject can be found in ref. [70]. It is interesting to notice that, at variance with A and Z, $y_p(\rho_B)$ plotted in the insert of Fig. II.3(b) shows no sensitivity to the equation of state. This means that the energetics of electrons dominates over the details of the nucleon-nucleon interaction. The significant difference in atomic number between our model (irrespective of the effective interaction) and the original Negele-Vautherin Hartree-Fock calculation [8] is due to the fact that our cluster model with the energy density functional [62] eq.(II.13) contains only the smooth part of the cluster energy. The neglected shell effects are responsible of the emergence of the magic number $Z = 40$ in the Hartree-Fock calculation. We can see that

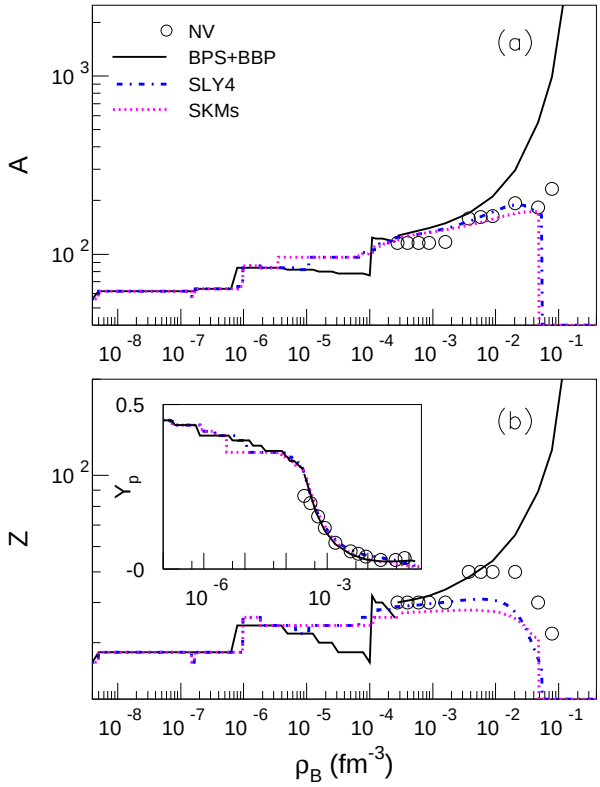

FIG. II.3: (Color online). Crust composition at T = 0: Baryonic (top panel) and atomic (lower panel) numbers of the equilibrium nucleus as a function of the baryonic density. NV stands for predictions by Negele and Vautherin [8]; BPS+BBP corresponds to predictions by BPS[1] and BBP[2] ; exp+SLY4(SKMs) stand for present model predictions when nuclear masses are calculated according to atomic mass data of Ref.[61] + LDM-SLY4 (SKMs) model of Ref.[62]. The inset in the bottom panel depicts the evolution with baryonic density of the total proton fraction.

the knowledge of shell closures for extremely neutron rich nuclei is much more important for the description of the inner crust than the isovector equation of state, and it is clear that to be predictive, the model at zero temperature should be augmented of realistic proton shell effects, as it is done in the Strutinsky approximation by S.Goriely and collaborators [68], at the obvious price of a greatly increased numerical effort. This limitation of eq.(II.13) will however not be a serious problem for the finite temperature applications for which the model has been conceived, and which will be studied in the second part of this paper.

The most striking feature of Fig.II.3 is the huge qualitative discrepancy at high density with the original inner crust BBP model [2]. To understand the origin of this difference Fig.II.4 displays the behavior as a function of the baryonic density of the mass of the energy-cluster [54] from eq.(II.6). We can see that the difference between BBP and our approach starts when the e-cluster size starts to depart from the r-cluster size, that is when the contribution of the neutron gas becomes important. In this situation one can expect a modification of the surface energy of the cluster according to eq.(II.4). In BBP, the in-medium modified surface energy is assumed to be a monotonically decreasing function of the gas density, independent of the isospin, exactly vanishing when the density of the gas reaches the density of the cluster [2]. In the language of the present paper, this happens when $A_e = 0$ (see eq.(II.6)). In such a condition BBP clusters are liquid drops with bulk only, and their size naturally diverges. However, this approach completely neglects the energy cost of the isospin jump at the cluster-gas interface. It is shown in refs. [60, 70], in the framework of the extended Thomas-Fermi theory, that the in-medium correction to the surface energy show a complex dependence on the isospin, and specifically behave very differently in symmetric nuclear matter and in the equilibrium with a pure neutron gas. Only in the case of symmetric nuclei immersed in a symmetric gas the transition to the homogeneous core can be seen as the simple vanishing of surface energy with diverging size of the nuclei; conversely, in the case of β-equilibrium matter, the inclusion of in-medium surface effects leads to a weak decrease of the average cluster size and a slightly advanced dissolution of clusters in the dense matter.

Finally, it is important to stress that results at densities higher than about one fifth of normal nuclear matter

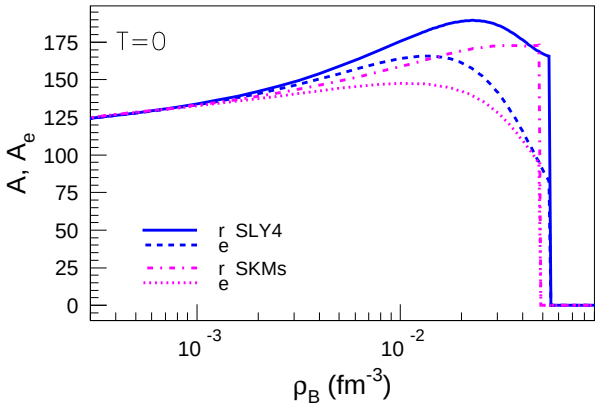

FIG. II.4: (Color online). Behavior of the cluster mass number as a function of the baryonic density in the inner crust using two different Skyrme functionals for both the free neutron energy density and the nuclear masses according to the LDM-Skyrme model of Ref. [62]. The total mass of the cluster is compared to the bound part of the cluster, obtained by simply subtracting the number of free neutrons according to eq.(II.6).

density are not reliable in any of the presented models because of the lack of deformation degrees of freedom which would allow the appearance of pasta phases [3, 4].

D. Equation of state

A quantity of primary importance when discussing the sensitivity of stellar matter energetics to the details of the nucleon-nucleon interaction or linking nuclear parameters with astronomical observables is the equation of state and, in particular, the total energy density - total pressure dependence.

The total energy density and pressure of the WS cell are plotted in Fig. II.5 as a function of baryonic density, in comparison with the result from the macroscopic BBP [2] and the microscopic Negele-Vautherin [8] model. We can see that the quantitative value of the energy density obviously depends on the model, and more specifically on the effective interaction, but in all cases over the considered density range the energy density surface is convex. This means that there is no way to minimize the system energy by state mixing, such that the system is thermodynamically stable. The discontinuous change of the crust composition due to the shell effects only leads to very tiny backbendings in the baryonic pressure as shown in the insert of Fig.II.5, and already observed by different authors [64–68]. These structures can be formally interpreted as phase transitions, but are so small that are not expected to have any thermodynamic consequence and can simply be understood as an interface effect.

The absence of a phase coexistence region covering a broad density domain, well known in the astrophysical context, is surprising from the nuclear physics viewpoint because it is in clear contrast with the phenomenology of pure baryonic matter, which is dominated at sub-saturation densities by the nuclear liquid-gas phase transition[73]. One may wonder if this difference is due to the fact that we are limiting our analysis to a limited part of the two-dimensional baryon density space that is explored in β-equilibrium. Indeed the β-equilibrium trajectory corresponds to very neutron rich matter, and it is well known that the coexistence zone in the nuclear matter phase diagram shrinks with increasing asymmetry. We therefore turn to demonstrate that the difference between stellar matter and nuclear matter thermodynamics is not restrained to β-equilibrium.

E. Phase transitions in the inner crust?

In the previous section we have assumed that a one-to-one correspondence exists between baryonic density and chemical potential, that is a unique Wigner-Seitz configuration can be systematically associated to each pressure and chemical potential field inside the star.

This is only correct in the absence of phase transitions, and it is in principle possible that a mixture of different Wigner-Seitz configurations might lead to a lower energy density than a periodic repetition of the same cell. The highly degenerate energy minima showed by the experimental energy surface even without the (more model dependent)

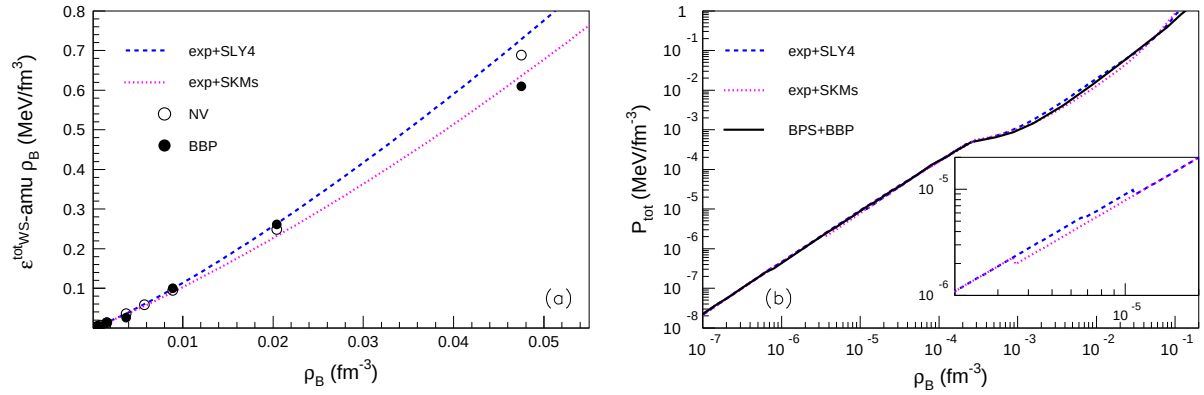

FIG. II.5: (Color online). Total energy density and total pressure as a function of baryonic density corresponding to the neutron star crust (T=0, β-equilibrium). Experimental [61] and LDM binding energies [62] have been used. The employed nuclear effective interaction are SLY4 and SKMs. Present results are confronted with those of NV [8] and BBP [2].

inclusion of unbound neutrons beyond the drip-lines (see figure II.1) evoke the possibility that first order phase transitions could even appear at finite temperature in the outer crust.

More generally, it is well known that such a first-order phase transition covers almost the whole phase diagram of sub-saturation neutral nuclear matter [73] and has baryonic density as order parameter. It is therefore natural to ask whether such a phase transition persists in the stellar context. As a matter of fact, the existence of such first order phase transition is systematically assumed in most seminal papers on the stellar matter equation of state[2, 5, 33], and in particular it is implemented in the publicly available and popularly used LS tables [35]. Even more modern equations of state of supernova matter[46, 71] invoke the persistence of the nuclear liquid-gas phase transition in the stellar context, based on the fact that the baryonic energy density of star matter is unstable with respect both to thermodynamical[73, 74] and to finite size density fluctuations[7, 72, 75].

On the other side, it was shown in different works that the liquid gas phase transition in stellar matter is quenched by the very strong incompressibility of the electron background [14, 74–77], and microscopic modelizations of the Wigner-Seitz cell have confirmed a continuous transition from the solid crust to the liquid core through a sequence of inhomogeneous pasta phases [13, 14, 18, 19, 26, 30–32, 34, 78, 79].

It is therefore important to examine this question in further detail.

We have already seen in section II C that the solution of eqs.(II.22)-(II.25) is always unique, even if many different solutions can be very close in energy per nucleon (see Figure II.1).

This means that at zero temperature a unique cluster-gas configuration can be associated to a given value of $\rho_B^{WS} = A_{WS}/V_{WS}$, $y_p^{WS} = Z_{WS}/A_{WS}$. This statement can of course be model dependent, as we have seen that very small variations of the mass functional can lead to very different results. However, even if multiple solutions of the cluster configuration would occur (which will indeed be the case at finite temperature), this would not lead to a first order phase transition. For a first-order phase transition to occur, solutions corresponding to different densities should be degenerate in (constrained) energy. Then, the absolute energy density minimum would be obtained by mixing these degenerate configurations with different ρ_B^{WS}, y_p^{WS}. If this was the physical result, the single-nucleus approximation would fail, and even at zero temperature one should account for a distribution of different Wigner-Seitz cells.

Thermodynamical instabilities and eventual phase transitions in systems with more than one component have in principle to be studied in the full N-dimensional density space [80]. In our case this means that the energy density has to be studied in the full two dimensional (ρ_n, ρ_p) plane, and the β-equilibrium condition has to be applied only after the Gibbs construction is performed (indeed β-equilibrium has to be imposed only at the macroscopic level, and can very well be violated at the microscopic level of a single cell). However the problem simplifies if the order parameter is known. In that case it is useful to introduce a Legendre transformation of the thermodynamical potential with respect to the chemical potentials of all the densities except the order parameter [73]. Then the multi-dimensional Gibbs construction exactly reduces to a one-dimensional Maxwell construction on the residual density.

In the case of stellar matter the neutrality condition $\rho_p = \rho_e$ allows a variable change $(\rho_n, \rho_p) \rightarrow (\rho_B = \rho_n + \rho_p, \rho_L = \rho_e)$. Due to the very huge electron incompressibility it is reasonable to expect that the two coexisting phases, if any, would not present any jump in electron density [75]. Microscopic calculations [14] have convincingly shown that the electron polarization by the proton distribution is negligible, as long as the clusters have linear dimensions of the order of the femtometer. Then, we can safely perform a Legendre transform with respect to ρ_L and introduce the

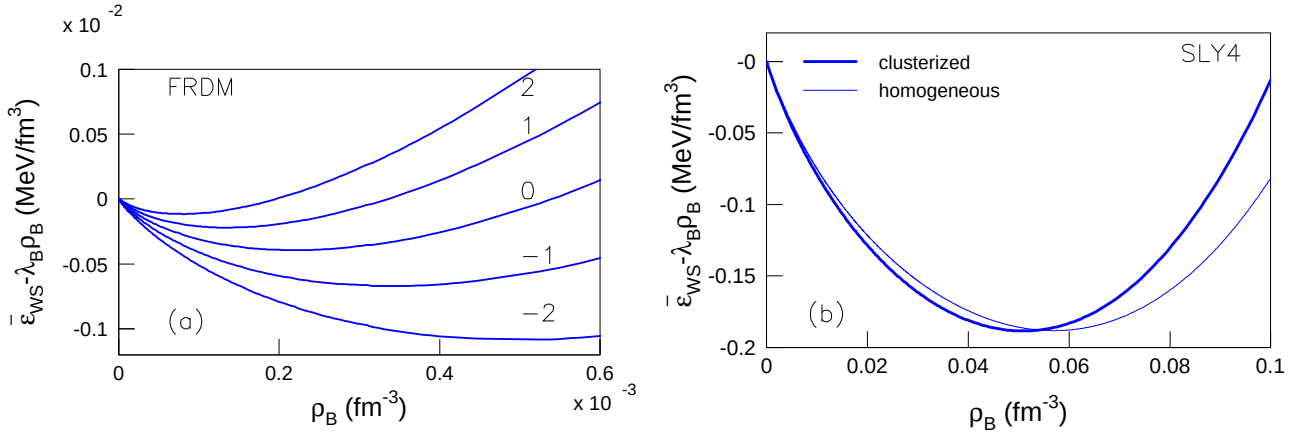

FIG. II.6: (Color online). Constrained energy densities as a function of density. Left: Outer crust as obtained using FRDM. The numbers accompanying the curves are in MeV and stand for λ_B. Right: Crust (thick line) and β-equilibrated homogeneous matter (thin line) at T=0 corresponding to SLY4 and $\lambda_B = 11.25$ MeV.

constrained energy density

$$\bar{\epsilon}_{WS}(\rho_B, \mu_L) = \epsilon_{WS}(\rho_B, \rho_L) - \mu_L \rho_L, \tag{II.36}$$

where μ_L stands for lepton chemical potential and ρ_L is the value taken by the lepton density at chemical potential μ_L, $\rho_L = \rho_L(\mu_L)$. Note that $\mu_L = 0$ corresponds to β-equilibrium in lack of neutrinos, $\mu_n^{tot} = \mu_p^{tot} + \mu_e^{tot}$. We do not therefore need to examine the whole μ_L plane, but can limit ourselves to the single point $\mu_L = 0$.

We can then conclude that we can identify the possible presence of phase transitions in the neutron star crust by simply considering the ρ_B density behavior of the energy density in β-equilibrium, $\epsilon_{WS}(\rho_B, \rho_L(\rho_B, \mu_L = 0))$. As in the previous chapter, ϵ_B is obtained solving, for each condition (ρ_B, y_p) the coupled equations (II.22)-(II.25).

To better evidence possible convexities, it is useful to introduce a linear bias

$$\bar{\epsilon}_{WS,\lambda_B}(\rho_B, \mu_L = 0) = \bar{\epsilon}_{WS}(\rho_B, \mu_L) - \lambda_B \rho_B. \tag{II.37}$$

The equilibrium solution of star matter corresponding to the chosen value of the external chemical potential field λ_B is given by the minimum of this function. If the function $\bar{\epsilon}_{WS}$ is convex, it will be characterized by a single mimimum value giving the usual relation between intensive and extensive variables

$$\lambda_B = \frac{\partial \epsilon_B}{\partial \rho_B} = \mu_B. \tag{II.38}$$

However, if $\bar{\epsilon}_{WS}$ has concave region(s) on the baryonic density axis ρ_B, it will be possible to find one or more values of λ_B such that two (or more) different configurations correspond to the same value of the constrained energy density. This will indicate a first order phase transition. The constrained energy density eq.(II.37) for clusterized matter in the crust is displayed in Fig. II.6 for some chosen values of λ_B corresponding to minima in the outer (left side) and inner (right side), respectively. We can see that both in the outer and inner crust the constrained energy surface is smooth and that the equilibrium configuration is given by a single Wigner-Seitz cell, thus justifying our variational procedure. To be able to analytically perform the derivatives in eqs. (II.22)-(II.25), we have switched to the Skyrme-LDM mass model [62] to produce the right panel. Again, a unique clusterized solution characterizes the equilibrium up to densities of the order of $\rho_0/5 - \rho_0/3$. At that value, it becomes possible to put in equilibrium clusterized and homogeneous matter. This defines a (tiny) region of first-order phase transition, much less extended than the liquid-gas phase transition of normal nuclear matter. Indeed this latter covers the whole sub-saturation density region. Moreover, this residual phase transition is an artifact of the present model which does not account for deformation degrees of freedom. It is well known that in this density domain deformed pasta structures correspond to the equilibrium configuration [6]. For this reason, we do not perform any Gibbs construction and simply put to zero the cluster mass at the transition point, assuming that pasta would take over. The results of Fig.II.6 show that the thermodynamics of $\beta-$ equilibrated matter is completely different from the one of nuclear matter.

As previously discussed in refs.[75] within mean-field arguments, this difference is due to the huge electron gas incompressibility which quenches the phase transition in stellar matter.

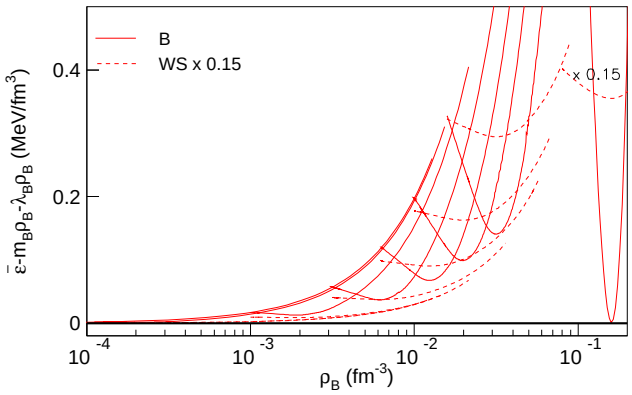

FIG. II.7: (Color online). Constrained energy density eq.(II.39) in the thermodynamic condition corresponding to the liquid-gas phase transition of symmetric matter, $\lambda_B = 15.95$ MeV. The different curves represent different values of the total proton density ρ_p. Solid (dashed) curves correspond to constrained baryonic (total) energy density. $m_B\rho_B$ stands for the rest mass contribution $(m_n\rho_n + m_p\rho_p)c^2$. The considered effective interaction is SLY4.

To demonstrate this point in the framework of the present model, we turn to consider the behavior of the baryonic part of the energy density $\epsilon_B = \epsilon_{WS} - \epsilon_{el}$ in the full (ρ_B, ρ_p) plane.

To better spot convexities in the two-dimensional space, we introduce again a constrained energy density

$$\epsilon_{\lambda_B,\lambda_3}(\rho_B, \rho_p) = \epsilon_B(\rho_B, \rho_p) - \lambda_B\rho_B - \lambda_3(\rho_B - 2\rho_p), \tag{II.39}$$

where λ_B and λ_3 represent an isoscalar and isovector external chemical potential field.

Again, phase transitions will be signalled by the existence of one or more values (λ_B, λ_3) such that two (or more) different configurations correspond to the same value of the constrained energy density.

In the case of uncharged nuclear matter, we know that the dominant part of the (λ_B, λ_3) plane is characterized by concavities. It is therefore not surprising to see that this is clearly the case for the ϵ_B function plotted in Fig. II.7.

This figure displays the energy density obtained solving the variational equations eqs.(II.22-II.25), biased by an external chemical potential field according to eq.(II.39). The value of the total proton density ρ_p is the same in each point of the different curves plotted in the figure. Because of the neutrality constraint $\rho_p = \rho_e$, each curve represents a given screening factor to the cluster Coulomb energy according to eq.(II.10). The minimum of each curve then gives the ensemble of optimal Wigner-Seitz cells corresponding to the chosen λ_3 value, and to different baryon density. The absolute minimum corresponds to the equilibrium Wigner-Seitz cell associated to the couple (λ_B, λ_3). The (N, Z) sequence of the corresponding cluster gives the composition, as a function of baryonic density, of matter at that λ_3 chemical potential.

The choice $\lambda_3 = 0$ selects the equilibrium solutions for symmetric matter. A unique point is the absolute minimum for all choices of λ_B except $\lambda_B = -15.95$ which is shown in the figure. At that chemical potential, if the electron part of the energy density is not taken into account (solid curves), two different points correspond to the same constrained energy. This corresponds to the well-known nuclear matter phase transition which at zero temperature takes place at a chemical potential equal to the saturation energy, $\mu_B = -15.95$ MeV for the SLY4 functional chosen in Fig. II.3. We can notice that the low density phase, which is predicted to be the vacuum phase in mean-field calculations, is obtained here at a low but finite density, corresponding to the most stable $N = Z$ isotope ^{56}Ni. This is due to the limitation of mean-field calculations that do not account for clusterization at low density.

In the stellar matter case, because of the Coulomb coupling between protons and electrons, the lepton part of the energy density is not independent of the baryon part. This means that the energy in the Wigner-Seitz cell has to include the electron zero point energy as written in eq.(II.3) . The total energy densities are given by dashed curves in Fig.II.3. This contribution is a simple constant shift of each curve because of the condition $\rho_p = \rho_e$, and therefore does not change the sequence of optimal compositions as a function of the density. From a thermodynamic point of view, we can say[77] that the canonical solution is the same as without the electron contribution. However, the electron energy density is a monotonically increasing function of $\rho_e = \rho_p$, and the optimal ρ_p monotonically increases with ρ_B in this symmetric matter situation we are considering. As a consequence, no value of λ_B can be found such that two different Wigner-Seitz cells can be put in equilibrium, and the phase transition disappears. This can be

easily understood mathematically considering that the optimal energy density gains an extra term as

$$\epsilon_B \to \epsilon_{WS} = \epsilon_B + \epsilon_{el}(\rho_p). \tag{II.40}$$

The relations (II.38) between density and chemical potential are shifted because of the electron contribution

$$\lambda_B \to \mu'_B = \mu_B + \frac{1}{2}\mu_{el} \;\; ; \;\; \lambda_3 \to \mu'_I = \mu_3 - \frac{1}{2}\mu_{el}, \tag{II.41}$$

and the curvature of the constrained energy density becomes:

$$\frac{\partial^2 \epsilon_\mu}{\partial \rho_B^2} = \frac{\partial \mu_B}{\partial \rho_B} + \frac{1}{2}\frac{\partial \mu_e}{\partial \rho_e}. \tag{II.42}$$

Because of the very high electron incompressibility, the convexity observed in the baryonic part of the energy density is not present any more in the total thermodynamic potential. This is known in the literature as the quenching of the phase transition due to Coulomb frustration[75, 76], and shows[77] that convexities in the (free) energy density do not necessarily correspond to instabilities in the physical system.

This shows that if one wants to formulate the equilibrium problem in the grandcanonical ensemble, one has to account for the electron zero point motion. This is a triviality for the zero-temperature problem, since the modelization in the Wigner Seitz cell is naturally done in the canonical ensemble. However, in the finite temperature NSE problem, which is typically treated grandcanonically, this kinetic contribution is usually disregarded with the argument that, the electrons being an ideal gas, the corresponding partition sum is factorized [46, 47]. It is then important to stress that a negative eigenvalue in the baryonic energy curvature matrix should not be taken as a sign of a first order phase transition: stellar matter inside the convex region is clusterized but perfectly stable, and no Maxwell or Gibbs constructions should be performed to get the equation of state.

We will come back on this point in the second part of this paper.

To summarize the results of this section, first order phase transitions could be possible in zero temperature stellar matter only if the function ϵ_{WS} defined in eq.(II.5), with the values of A, I, ρ_g, V_{WS} obtained from eqs.(II.22)-(II.25), presents a convexity anomaly as a function of ρ_B^{WS}, for fixed values of ρ_p. As it can be seen in Figs.II.6, II.7, this is not the case even using energy functionals for the nuclear masses which include shell effects. In particular, the minimum of the constrained energy density for a given set of chemical potential is systematically associated to a single Wigner-Seitz cell, characterized by a unique composition in terms of cluster and gas mass and composition. This means that the SNA is perfectly adequate to deal with the zero temperature problem.

III. FINITE TEMPERATURE STELLAR MATTER

In the second part of this paper we extend to the finite temperature regime the modeling of the Wigner-Seitz cell with cluster degrees of freedom, presented in the first part. We will start by deriving the classical equations corresponding to the single nucleus approximation. This approach is at the origin of most extensively used equations of state for supernova matter[35, 36]. Then the main part of the paper is devoted to the derivation of an extended nuclear statistical equilibrium model, which by construction reproduces the results of SNA if only the most probable cluster is considered, and the same chemical potentials are considered. Since the SNA naturally converges at T=0 to the standard modelization of the neutron star crust, the consistency between the theoretical treatment of neutron star crust and finite temperature supernova matter will thus be guaranteed.

A. Single nucleus approximation

The natural extension at finite temperature of the model presented in the first part of this paper consists in keeping the SNA approach, and replace the variational problem of the energy density minimization with the variational problem of the free energy density minimization. In the e-cluster representation eq.(II.3) the energy is additive and we can write for a given configuration $k = \{V_{WS}^{(k)}, A^{(k)}, \delta^{(k)}, \rho_g^{(k)}, y_g^{(k)}\}$

$$F_{WS} = F_\beta^e(A, \delta, \rho_g, y_g) - TV_{WS} \ln z_\beta^{HM}(\rho_g, y_g) - TV_{WS} \ln z_\beta^{el}(\rho_p) + \delta F_{surf}, \tag{III.1}$$

where z_β^{HM} is the mean-field partition sum for homogeneous matter. The electron contribution is independent of the different configurations and the associated partition sum z_β^{el} will be factorized out. Similar to the previous section,

we will neglect the surface in-medium corrections to the free energy, though they might turn out to be important in the situations where the gas contribution is not negligible.

If we consider temperatures higher than the solid-gas phase transition temperature, the free energy of a cluster (A,δ) is different from its ground state energy because at finite temperature the cluster can be found in different translational and internal states.

To calculate this term, one has to consider that within the A_{WS} total number of particles, a number $A_g = \rho_g V_{WS}$ belongs to the gas part. The entropy associated to these particles is already contained in the term $\ln z_\beta^{HM}$. To avoid a double-counting of the number of states, the canonical partition sum of the cluster must thus be defined summing up the statistical weight of the different energy states associated to this reduced particle number (see eqs.(II.6),(II.7)):

$$Z_{WS}^{cl}(A,\delta,\rho_g,y_g) = \sum_{\vec{p}}\sum_{E^*} \exp -\beta\left(\frac{p^2}{2mA_e} + E^e + E^*\right). \tag{III.2}$$

The cluster center-of-mass motion is a plane wave. The first sum is thus given by the plane wave density of states, with periodic boundary conditions at the cell borders. This is simply

$$\sum_{\vec{p}} = \frac{V_{WS}}{(2\pi\hbar)^3}\int d^3p. \tag{III.3}$$

Notice that the available volume for the center of mass is the whole Wigner-Seitz volume, and there is no excluded volume effect. The center-of-mass momentum integral is a Gaussian integral

$$\int d^3p \exp -\beta\frac{p^2}{2mA_e} = \left(\frac{2\pi m A_e}{\beta}\right)^{3/2}. \tag{III.4}$$

The sum over the cluster excited states has to be cut at the average particle separation energy, to avoid double counting with the gas states. This leads to a temperature dependent degeneracy factor defined by:

$$\sum_{E^*} \exp -\beta E^* = \int_0^{<S>} dE \rho_{A,\delta}(E) \exp -\beta E^* = g_\beta(A,\delta,\rho_g,y_g), \tag{III.5}$$

where $< S >= \min(< S_n >, < S_p >)$ is the average particle separation energy. For the numerical applications of this paper, we will use for simplicity a different higher energy cut-off for each cluster species $< S > \approx < S > (A,\delta,\rho_e) = \min(< S_n > (A,Z,\rho_e), < S_p > (A,Z,\rho_e))$, with separation energies calculated from the smooth part of the cluster energy functional, given by $E_{LDM}^{vac} + \delta E_{coul}$.

In the zero temperature limit $g_\beta \to g_{GS} = 2J_{GS}+1$ gives the spin degeneracy of the cluster ground state. For the numerical applications of this section, in order to have analytically differentiable functions, we have systematically used the Skyrme-LDM model for nuclear mass [62] and a simple Fermi gas level density for $\rho_{A,\delta}(E)$ [47]. A more realistic choice will be presented in section III C.

The cluster free energy in the Wigner Seitz cell then reads

$$\begin{aligned} F_\beta^e &= -T\ln Z_{WS}^{cl} = F_\beta^0 + T\ln z_\beta^{HM}(\rho_g,y_g)\frac{A}{\rho_0} \\ &= E^e(A,\delta,\rho_g,y_g,\rho_p) - T\ln V_{WS} - T\ln c_\beta - \frac{3}{2}T\ln A_e \end{aligned} \tag{III.6}$$

with $c_\beta = g_\beta(mT/(2\pi\hbar^2))^{3/2}$, and m the nucleon mass .

The auxiliary function to be minimized is the extension of eq.(II.18) including the entropy terms:

$$\begin{aligned} \mathcal{D}_\beta(A,\delta,\rho_g,y_g,V_{WS}) &= \frac{F_{WS}(A,\delta,\rho_g,y_g,\rho_p)}{V_{WS}} \\ &- \alpha\rho_g\left(\rho_0 - A/V_{WS}\right) + \alpha\rho_0\left(\rho_B - A/V_{WS}\right) \\ &- \beta y_g\left(\rho_0 - A/V_{WS}\right) + \beta\rho_0\left(\rho_B(1-2y_p) - A\delta/V_{WS}\right). \end{aligned} \tag{III.7}$$

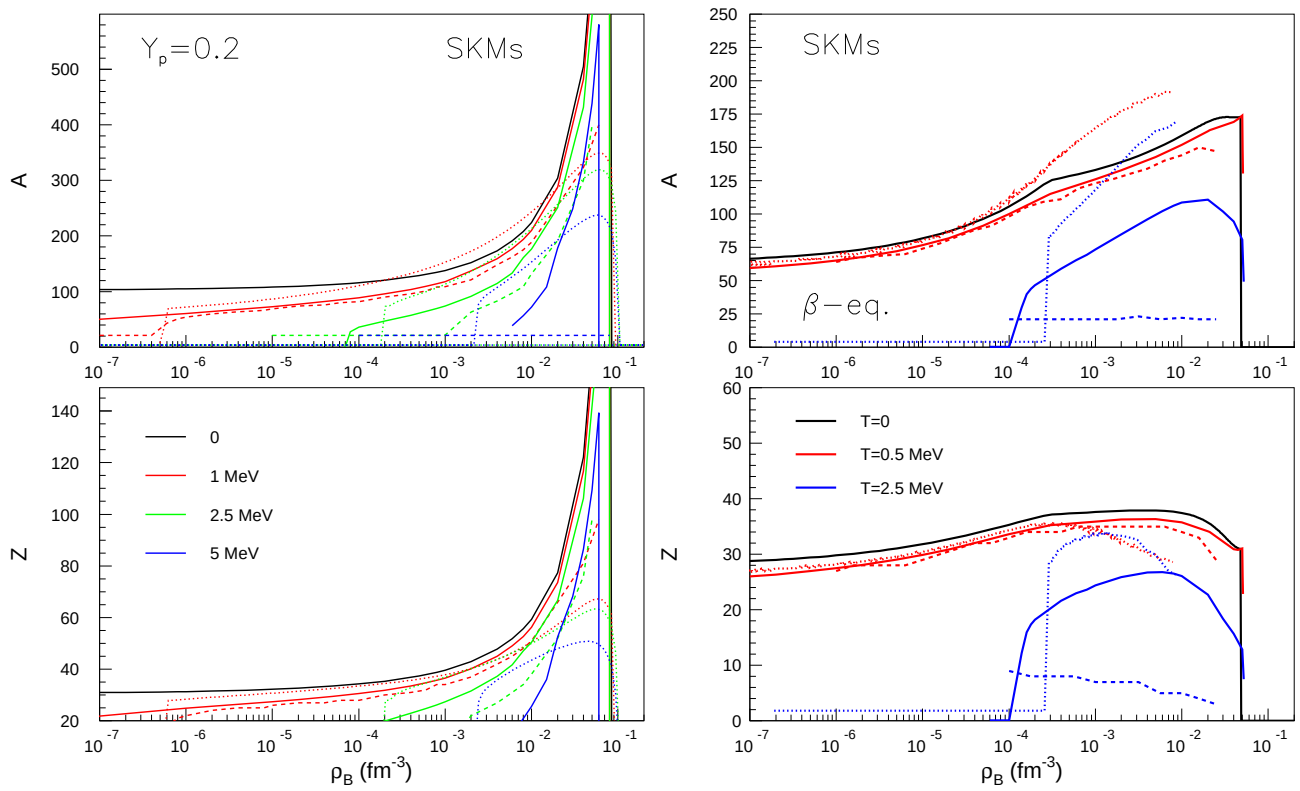

FIG. III.1: (Color online). Mass (top panel) and atomic (bottom panel) numbers of the unique nucleus of the WS cell as a function of baryonic density. Left side: Y_p=0.2 and different temperatures $T = 0, 1, 2.5, 5$ MeV. Right side: β-equilibrium and different temperatures $T = 0, 0.5, 2.5$ MeV. Present SNA model (thick lines) is compared with the LS results [35] corresponding to LS220 as calculated in Ref. [83] (thin lines) as well as with the NSE prediction for the most probable cluster (dashed lines). The LDM-SKMs model of ref.[62] is used for the cluster energy functional.

The variational equations result:

$$\frac{\partial E^e}{\partial A}|_{\delta,\rho_g,y_g} = \mu_B\frac{\rho_0-\rho_g}{\rho_0}+\mu_3\frac{\rho_0\delta-y_g}{\rho_0}+\frac{3T}{2A}\frac{\rho_0 V_{WS}}{\rho_0 V_{WS}-A}+T\frac{\partial \ln c_\beta}{\partial A}|_{\delta,\rho_g,y_g}, \tag{III.8}$$

$$\frac{\partial E^e}{\partial \delta}|_{A,\rho_g,y_g} = \mu_3 A+\frac{\rho_0' A}{\rho_0}(\mu_B\frac{\rho_g}{\rho_0}+\mu_3\frac{y_g}{\rho_0})+\frac{3}{2}T\frac{\rho_0'\rho_g V_{WS}}{(\rho_0-\rho_g)(\rho_0 V_{WS}-A)}+T\frac{\partial \ln c_\beta}{\partial \delta}|_{A,\rho_g,y_g}, \tag{III.9}$$

$$\frac{\partial(F_\beta^0/A)}{\partial A}|_{\delta,V_{WS}} = 0, \tag{III.10}$$

$$\mu_B \equiv -T\frac{\partial \ln z_\beta^{HM}}{\partial \rho_g} \tag{III.11}$$

$$\mu_3 \equiv -T\frac{\partial \ln z_\beta^{HM}}{\partial y_g}. \tag{III.12}$$

The finite temperature predictions of SNA are plotted in Figs. III.1 for different density, temperature and proton fraction conditions.

As expected, a monotonic decrease of the cluster size as a function of temperature is obtained at constant proton fraction, and the results converge for $T \to 0$ to our zero temperature results in the Wigner-Seitz cell, which we know to be exact at the thermodynamic limit, and model independent below neutron drip. The non-monotonic behavior with density observed in β-equilibrium is due to the strong decrease of proton fraction with increasing density, which finally leads to the dissolution of clusters in homogeneous matter when the proton fraction becomes so low that loosely bound hydrogen and helium resonances dominate over heavy clusters. At constant proton fraction this effect is not apparent, meaning that the in-medium bulk energy shift is not enough to suppress the cluster binding. In that

case, the preferential cluster size monotonically increases with density up to the point where homogeneous matter is energetically prefered. As in the previous section, we have indicated that point by putting to zero the $A(\rho_B)$ and $Z(\rho_B)$ curves.

We cannot exclude that the inclusion of surface in-medium effects, neglected in this paper, could change this behavior. However preliminary results[70] indicate that this effect is small.

The qualitative behavior of the cluster size and charge with density is similar to the one of the LS220 Lattimer-Swesty equation of state, plotted with dotted lines in Fig.III.1. Quantitative differences exist nevertheless. On one hand they are trivially due to the different employed cluster energy functional. In terms of properties of saturated symmetric nuclear matter SKMs is characterized by $J_{sym} = 30.06$ MeV, $L_{sym} = 45.8$ MeV, $K_{sym} = -156$ MeV, $K_{sat} = 216.7$ MeV while LS200 has $J_{sym} = 29.3$ MeV, $L_{sym} = 74$ MeV, $K_{sym} = 64.9$ MeV, $K_{sat} = 220$ MeV. While the compressibility (K_{sat}) of symmetric matter is comparable for the two functionals, they differ in the slope (L_{sym}) and curvature of the symmetry energy (K_{sym}), which can influence the cluster size [70] in an important way for neutron rich matter. This discrepancy is hard to remove since the Skyrme-LDM model we have used for nuclear masses does not include any Skyrme interaction sufficiently similar to LS220. Probably more important, the SNA model of Lattimer-Swesty additionally accounts for alpha-particles that can be present in the WS cell together with heavier clusters. The presence of an isospin-symmetric bound component in the gas obviously modifies the cluster size and composition. Finally, to obtain the emergence (at low density) and dissolution (at high density) of clusters, first order phase transitions to an α particle gas and to homogeneous matter respectively, are implemented in the LS model[35].

We will discuss in section III C that the inclusion of the proper statistical weight of clusters of all sizes naturally leads to the emergence of an important fraction of light particles, and to the disappearance of heavy nuclei in the dense medium, without invoking any phase transition. We also note that at the highest temperatures, our SNA clusters tend to be smaller than in LS. This is probably due to the high energy cut in the density of state integral eq.(III.5) implemented in order to avoid double counting of the continuum states, which reduces the statistical weight of heavy clusters.

In the treatment of finite temperature we have presented in this section we have assumed that, similar to the zero temperature case, stellar matter in a given thermodynamic condition (ρ_B, y_p, T) is characterized by a single well defined Wigner-Seitz cell. This is of course an approximation, since what has to be minimized at equilibrium is the total free energy density, and not the single-cell free energy density. The two variational approaches will give approximately the same result if the free-energy landscape has a single deep minimum, but if different Wigner-Seitz cells correspond to comparable free energies, they will all be present in the equilibrium configuration, even if with different probabilities. As we could have anticipated from inspection of Fig.II.1, the free energy landscape is highly degenerate for stellar matter. This is shown for two arbitrary representative thermodynamic conditions in Fig.III.2, which shows the free energy densities of different Wigner-Seitz cells, which correspond to different nuclei all of them immersed in the same neutron, proton and electron gas. At the lowest considered temperature we can see that, though a single minimum exists, which corresponds to the solution of the SNA variational coupled equations (III.8)-(III.12) for this given set of constraints, different (heavy as well as light) nuclei might lead to comparable free energy densities, and will therefore be present at equilibrium. The higher considered temperature shows a different pattern. Indeed, a plethora of nuclei with masses and isospin symmetries spanning important ranges have close values of the constrained free energies. It is easy to anticipate that if pairing and shell effects were ignored, the minimum of the contrained free energy would have been even flatter.

B. Thermodynamic limit in the canonical ensemble

The very principle of statistical mechanics tells us that at non-zero temperature different realizations of the Wigner-Seitz cell will be possible within the same constraint of total density and proton fraction.

If we consider a very large volume V which contains a number $n \to \infty$ of different Wigner-Seitz cells for a total number of particles A_{tot} and a total isospin asymmetry I_{tot}, a possible realization of the system is now characterized by $k = \{n_i^{(k)}, i = 1, \ldots, \infty\}$ where $n_i^{(k)}$ is the number of realizations, within the volume V, of an arbitrary Wigner-Seitz cell constituted of a cluster with particle numbers $A_e^{(i)}, I_e^{(i)}$ and a gas with particle numbers $A_g^{(i,k)} = V_{WS}^{(i)} \rho_g^{(k)}, I_g^{(i,k)} = V_{WS}^{(i)} y_g^{(k)}$. Notice that the gas density and isospin can in principle depend on the realization (k) but do not depend on the cell (i). Indeed the nucleon gas density is uniform over the volume because we have divided it in cell only for convenience, and the variation of gas particle numbers is just due to the variation of Wigner-Seitz volumes.

The total number of particles in the cell $A_{WS}^{(i)}, I_{WS}^{(i)}$ varies from one cell to the other, but the total number of

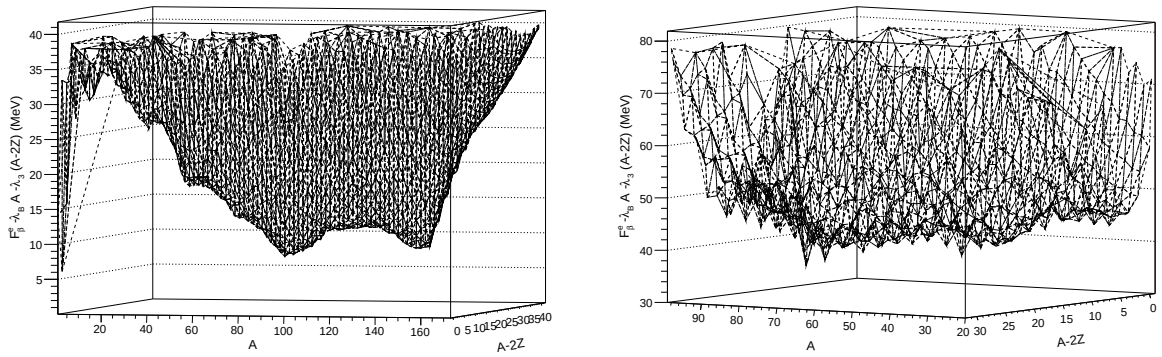

FIG. III.2: (Color online). Surface of cluster constrained free energy corresponding to $\rho_B = 10^{-3}$ fm^{-3}, Y_e=0.39 and T=0.5 MeV (left) and, respectively, 2.4 MeV (right). The values of (λ, λ_3) are (-10.06 MeV, 3.98 MeV) and, respectively, (-11.03 MeV, 5.86 MeV). Experimental values [61] and predictions of the 10-parameter mass model of Duflo-Zuker[82] have been used for the binding energies.

particles in the volume V

$$A_{tot} = \sum_i n_i^{(k)}(A_e^{(i)} + V_{WS}^{(i)}\rho_g^{(k)}), \tag{III.13}$$

$$I_{tot} = \sum_i n_i^{(k)}(I_e^{(i)} + V_{WS}^{(i)}y_g^{(k)}), \tag{III.14}$$

$$V = \sum_i n_i^{(k)}V_{WS}^{(i)}. \tag{III.15}$$

is the same for each realization (k). Since we are at the thermodynamic limit, these three conditions are in reality only two

$$\rho_B = \frac{A_{tot}}{V} = \frac{\sum_i n_i^{(k)}(A_e^{(i)} + V_{WS}^{(i)}\rho_g^{(k)})}{\sum_i n_i^{(k)}V_{WS}^{(i)}}, \tag{III.16}$$

$$y_B = \frac{I_{tot}}{V} = \frac{\sum_i n_i^{(k)}(I_e^{(i)} + V_{WS}^{(i)}y_g^{(k)})}{\sum_i n_i^{(k)}V_{WS}^{(i)}}. \tag{III.17}$$

We can then characterize a realization (k) by the fragment distribution and the gas densities $k = \{n_i^{(k)}, i = 1, \ldots, \infty, \rho_g^{(k)}, y_g^{(k)}\}$ where now $n_i^{(k)}$ is the number of occurrences of the Wigner-Seitz cell (i) constituted of a gas $\rho_g^{(k)}, y_g^{(k)}$, a cluster $A_e^{(i)}, I_e^{(i)}$ and a volume $V_{WS}^{(i)}$ uniquely defined by the neutrality condition which has to be fulfilled in each cell

$$\frac{Z_e^{(i)} + V_{WS}^{(i)}\rho_{gp}^{(k)}}{V_{WS}^{(i)}} = \rho_p = \frac{\rho_B - y_B}{2}. \tag{III.18}$$

We can further simplify the problem considering that, for a given macroscopic set of constraints (β, ρ_B, y_B) we will have a unique partitioning in the macroscopic volume between the cluster fraction and the gas fraction, that is the one that minimizes the total free energy. It is very easy to improve on this approximation if necessary, by considering the canonical probability associated to each partitioning. We do not do it because it comes out that there are very few combinations of $\rho_{clus} = \sum_i n_i A_e^{(i)}/V$ and ρ_g which lead to the same ρ_B. This means that we consider that ρ_g and y_g do not depend on (k) but only on the macroscopic constraints. Then the conservation law simplifies to:

$$\rho_B = \frac{A_{tot}}{V} = \frac{1}{V}\sum_i n_i^{(k)}A_e^{(i)} + \rho_g = \rho_{clus} + \rho_g, \tag{III.19}$$

$$y_B = \frac{I_{tot}}{V} = \frac{1}{V}\sum_i n_i^{(k)}I_e^{(i)} + y_g = y_{clus} + y_g; \tag{III.20}$$

and the different realizations of the set of constraints $(\beta, \rho_B, y_B, \rho_g, y_g)$ are defined by $k = \{n_i^{(k)}, i = A_e^{(i)}, I_e^{(i)}\}$.

The probability $p_\beta(k)$ of this realization is determined by the usual maximization of the information entropy under the constraint of the average energy and a sharp constraint on the mass A_{tot} and isospin I_{tot} eqs.(III.19),(III.20). We define the total free energy of each realization (k) as:

$$F_{tot}(k) = F_{clus}(k) - TV \ln \left(z_\beta^{HM}(k) z_\beta^{el} \right), \tag{III.21}$$

with

$$F_{clus}(k) = \sum_i n_i^{(k)} F_\beta^e(i); \tag{III.22}$$

$$F_\beta^e(i) = E^e(A, \delta, \rho_g, y_g, \rho_p) - T \ln V - T \ln c_\beta - \frac{3}{2} T \ln A_e. \tag{III.23}$$

It is interesting to remark that the cluster free energy at the thermodynamic limit eq.(III.23) differs from the cluster free energy in the Wigner-Seitz cell eq.(III.6). Indeed the number of states for the center-of-mass motion has to be calculated over the whole volume:

$$\sum_{\vec{p}} \exp -\beta \frac{p^2}{2mA_e} = \frac{V}{(2\pi\hbar)^3} \left(\frac{2\pi m A_e}{\beta} \right)^{3/2}. \tag{III.24}$$

This is well known from solid state physics and leads to the Bloch theorem: even if the ions are localized at fixed positions in the coulomb lattice, their center of mass motion is a plane wave over the whole volume[84, 85].

Thanks to the thermodynamic limit, the partition sums are now factorized

$$Z_\beta(\rho_B, y_B, \rho_g, y_g) = \sum_k \exp -\beta F_{clus}(k) \left(z_\beta^{HM} z_\beta^{el} \right)^V. \tag{III.25}$$

The probability of realization (k) is then simply given by:

$$p_\beta(k) = \frac{1}{Z_\beta^{clus}(\rho_B, y_B, \rho_g, y_g)} \exp -\beta F_{clus}(k), \tag{III.26}$$

with

$$Z_\beta^{clus} = \sum_k \exp -\beta F_{clus}(k). \tag{III.27}$$

We note by passing that we can easily extend this result to the case where we allow mixing of different ρ_g, y_g by considering eq.(III.25) as a constrained partition sum. In that case, the total partition sum has to be defined as

$$Z_\beta(\rho_B, y_B) = \sum_I Z_\beta^{clus}(\rho_B, y_B, \rho_g^I, y_g^I) \left(z_\beta^{HM}(\rho_g^I, y_g^I) \right)^V \left(z_\beta^{el} \right)^V. \tag{III.28}$$

Z_β^{clus} is the canonical partition sum of an ensemble of fully independent clusters, for a total mass number $A_{clus} = V\rho_{clus}$ and isospin $I_{clus} = V y_{clus}$. This is a classical problem[47, 86], and its solution is given by:

$$Z_\beta^{clus}(A_{clus}, I_{clus}, \rho_g, y_g) = \sum_{(k)} \prod_{A,Z} \frac{\left(\omega_\beta^e(A, Z) \right)^{n_{A,Z}^{(k)}}}{n_{A,Z}^{(k)}!}, \tag{III.29}$$

where

$$\omega_\beta^e(A, Z) = \exp -\beta F_\beta^e(A, \delta, \rho_g, y_g), \tag{III.30}$$

the sum runs over all possible realizations of the system such that the total number of particles is A_{clus}, $n_{A,Z}^{(k)}$ is the number or occurrences of cluster A, Z in the realization k, and the product runs over r-clusters A, Z or e-cluster A_e, Z_e equivalently, since the two are scaled by a factor which is constant if ρ_g, y_g are constant. This partition sum can be calculated with a Monte-Carlo technique[47] or also analytically via a recursive relation[77, 86].

Notice that for a finite system the total volume $V_{tot} = \sum_i n_i^{(k)} V_i$ is a fluctuating quantity, and only A_{clus} is the same event by event. However this is a not problem, because the conservation law is applied to the total density.

It is instructive to consider the SNA limit of a representative cluster. Let us suppose that the average multiplicity density $< n_{AZ} > /V \approx 1/ < V_{WS}(A, Z, \rho_B, y_B, \rho_g, y_g) >$ for a given $A = \bar{A}, Z = \bar{Z}$ and $< n_{AZ} > \approx 0 \; \forall A \neq \bar{A}, Z \neq \bar{Z}$, or equivalently let us suppose that we consider only the most probable cluster in the partition sum. Since $A_{clus} = n\bar{A}, I_{clus} = n(\bar{A} - 2\bar{Z})$ we immediately get

$$Z_\beta^{clus}(n\bar{A}, n\bar{Z}) = \frac{\left(\omega_\beta^e(\bar{A}, \bar{Z})\right)^n}{n!}, \tag{III.31}$$

and

$$\ln z_\beta^{clus}(n\bar{A}/V, n\bar{Z}/V) = \frac{1}{V_{WS}} \ln \frac{\omega_\beta^e(\bar{A}, \bar{Z})}{n}, \tag{III.32}$$

where we have used the Stirling approximation $\ln n! \approx n \ln n$ and introduced the free energy densities as $\ln z_\beta = \ln Z_\beta / V$. Using eq.(III.25) and eq.(III.6) the partition sum becomes

$$-T \ln z_\beta(\rho_B, y_B) = \frac{1}{V_{WS}} F_{WS}(\bar{A}, \bar{Z}, \rho_g, y_g). \tag{III.33}$$

We can see that we recover a SNA expression which we have already shown converges towards the exact result at zero temperature.

The value of $\bar{A}, \bar{Z}$ can be deduced from the equations of state

$$\mu_B = -T \frac{\partial \ln z_\beta}{\partial \rho_B}|_{y_B}; \tag{III.34}$$

$$\mu_3 = -T \frac{\partial \ln z_\beta}{\partial y_B}|_{\rho_B}, \tag{III.35}$$

which can also be written as

$$0 = \frac{\partial(-T \ln z_\beta - \mu_B \rho_B)}{\partial \rho_B}|_{y_B}; \tag{III.36}$$

$$0 = \frac{\partial(-T \ln z_\beta - \mu_3 y_B)}{\partial y_B}|_{\rho_B}. \tag{III.37}$$

Integrating these equations leads to:

$$d\left(-T \ln z_\beta - \mu_B \rho_B - k(y_B)\right) = 0; \tag{III.38}$$

$$d\left(-T \ln z_\beta - \mu_3 y_B - h(\rho_B)\right) = 0, \tag{III.39}$$

or also

$$d\left(-T \ln z_\beta - \mu_B \rho_B - \mu_3 y_B\right) = 0. \tag{III.40}$$

This is exactly the same minimization problem as in section IVa, with the difference that now the variables are A, δ, V_{WS} because ρ_g, y_g are fixed. This physically means that the fact of considering a large number of Wigner Seitz cell has eliminated the conservation constraint between A, δ and ρ_g, y_g: density and isospin fluctuations are allowed in each Wigner-Seitz cell because the conservation law applies only to the macroscopic system.

As a consequence, the equilibrium sharing equations are slightly modified:

$$\frac{\partial E^e}{\partial A}|_{\delta,\rho_g,y_g} = \mu_B \frac{\rho_0 - \rho_g}{\rho_0} + \mu_3 \frac{\rho_0 \delta - y_g}{\rho_0} + \frac{3T}{2A} + T \frac{\partial \ln c_\beta}{\partial A}|_{\delta,\rho_g,y_g}; \tag{III.41}$$

$$\frac{\partial E^e}{\partial \delta}|_{A,\rho_g,y_g} = \mu_3 A + \frac{\rho_0' A}{\rho_0}(\mu_B \frac{\rho_g}{\rho_0} + \mu_3 \frac{y_g}{\rho_0}) + \frac{3}{2} T \frac{\rho_g \rho_0'}{\rho_0(\rho_0 - \rho_g)} + T \frac{\partial \ln c_\beta}{\partial \delta}|_{A,\rho_g,y_g}, \tag{III.42}$$

with

$$\mu_B \equiv \frac{\partial f_g}{\partial \rho_g}; \tag{III.43}$$

$$\mu_3 \equiv \frac{\partial f_g}{\partial y_g}. \tag{III.44}$$

We can also notice that in the limit $T \to 0$ the sharing equations at $T = 0$ that we have obtained, by imposing exact conservation laws within the cells, are recovered as they should. Indeed in this limit the system is periodic and the global conservation law is equivalent to a local (within the cell) conservation law.

C. the grandcanonical NSE

The canonical treatment of the previous section is formally correct, but has the disadvantage of being extremely expensive from the computational point of view. For this reason, a grandcanonical formulation appears more appealing and has been preferentially invoked in the star matter literature[41–43, 45, 46, 48, 49].

To formulate this problem, we consider a very large volume $V \to \infty$ which contains a number $n \to \infty$ of a-priori different Wigner-Seitz cells, and introduce two external Lagrange multipliers to impose the average isoscalar and isovector densities over the whole volume. As in the previous section, a possible realization of the system is noted by an index $k = \{n_i^{(k)}, i = 1, \dots, \infty\}$ where n_i is the number of occurrences, within the volume V, of an arbitrary Wigner-Seitz cell constituted of a cluster with particle numbers $A^{(i)}, I^{(i)}$ and a gas with particle numbers $A_g^{(i)} = V_{WS}^{(i,k)} \rho_g^{(k)}, I_g^{(i)} = V_{WS}^{(i,k)} y_g^{(k)}$. The total number of particles in the cell $A_{WS}^{(i)}, I_{WS}^{(i)}$ varies from one cell to the other, but the total number of particles in the volume V (or more precisely, the total density and proton fraction, since we are at the thermodynamic limit $V \to \infty$), are fixed by the externally imposed chemical potentials μ_B and μ_3. These densities, as well as the average cluster multiplicities $< n_i >_{\beta\mu\tilde{\mu}}$ and the gas densities $< \rho_g >, < y_g >$, is what we want to calculate.

As we have already discussed, the gas density and isospin could in principle depend on the realization (k) but do not depend on the cell (i). The Wigner-Seitz volume is uniquely defined by the neutrality condition eq.(III.18) in the cell

$$V_{WS}^{(i,k)} = \frac{Z^{(i)}}{\rho_p - \rho_{gp}^{(k)}}. \tag{III.45}$$

The total Helmholtz free energy of each realization (k) is given by eq.(III.21):

$$F_{tot}(k) = \sum_i n_i^{(k)} \left(F_\beta^e(i) - T V_{WS}^{(i,k)} \ln \left(z_\beta^{HM}(k) z_\beta^{el}(\rho_p) \right) \right). \tag{III.46}$$

We can see that, because of the dependence on ρ_p of the electron free energy, this equation defines a self-consistency problem. Indeed we have:

$$\rho_p = \sum_i n_i^{(k)} \frac{Z_e^{(i)} + \rho_{gp}^{(k)} V_{WS}^{(i,k)}}{V}, \tag{III.47}$$

showing that our variational variables $\{n_i^{(k)}\}$ are not independent variables. As it is well known in the framework of the self-consistent mean-field theory [87], an equivalent one-body problem can be formulated corresponding to the same information entropy, therefore to the same set of occupations as in the self-consistent problem, but with a different free energy corresponding to independent particles, which contains rearrangement terms. These rearrangement terms will explicitly appear in the one-body occupations of the self-consistent problem. The free energy of the equivalent one-body problem is given by:

$$F_{tot}^{1b}(k) = -TV \ln z_\beta^{el}(\rho_p) + \sum_i n_i^{(k)} F_\beta^{1b}(i), \tag{III.48}$$

with

$$F_\beta^{1b}(i) = \frac{\partial F_{tot}}{\partial n_i^{(k)}} = F_\beta^e(i) - T V_{WS}^{(i,k)} \ln z_\beta^{HM}(k) + \mu_{el} \left(Z_e^{(i)} + \rho_{gp}^{(k)} V_{WS}^{(i,k)} \right), \tag{III.49}$$

where the derivation is taken at constant $\rho_g, y_g, n_j^{(k)}, j \neq i$. The grand-canonical occupations $n_i^{(k)}$ are determined by the free energy of the equivalent one-body problem, meaning that they directly depend on the electron chemical potential. Notice that in principle also $F_\beta^e(i)$ depends on the total proton density through the Coulomb screening term, therefore it should also give rise to extra rearrangement terms. However this extra term $\partial F_\beta^e / \partial \rho_p \cdot \partial \rho_p / \partial n_i \propto V^{-1}$, is negligible in the thermodynamic limit. The total Gibbs one-body free energy of each realization (k) is obtained by Legendre transformation with respect to the total baryon number and isospin. This amounts to introducing as usual two chemical potentials μ_B', μ_3' according to:

$$G_{tot}^{1b}(k) = F_{tot}^{1b}(k) - \sum_i n_i^{(k)} \left(\mu_B' A_{WS}^{(i)} - \mu_3' I_{WS}^{(i)} \right) \tag{III.50}$$

We can see that we can define auxiliary chemical potentials as

$$\mu_B = \mu'_B - \mu_{el}/2 \;\; ; \;\; \mu_3 = \mu'_3 + \mu_{el}/2 \tag{III.51}$$

such as to make formally disappear the electron contribution in the cluster free energy:

$$G^{1b}_{tot}(k) = -TV \ln z^{el}_\beta + \sum_i n^{(k)}_i \left(F^e_\beta(i) - TV^{(i,k)}_{WS} \ln z^{HM}_\beta(k) - \mu_B(A^{(i)}_e + V^{(i,k)}_{WS}\rho^{(k)}_g) - \mu_3(I^{(i)}_e + V^{(i,k)}_{WS} y^{(k)}_g) \right) \tag{III.52}$$

Using the mean-field relations of uniform nuclear matter:

$$\ln z^{HM}_{\beta\mu_B\mu_3} = \ln z^{HM}_\beta(\rho_g, y_g) + \beta\mu_B\rho_g + \beta\mu_3 y_g. \tag{III.53}$$

we can see that the gas densities are uniquely determined by the external chemical potentials, and independent of the realization, as we could expect:

$$\rho_g = T \frac{\partial \ln z^{HM}_{\beta\mu_B\mu_3}}{\partial\mu_B}|_{\mu_3}; \tag{III.54}$$

$$y_g = T \frac{\partial \ln z^{HM}_{\beta\mu_B\mu_3}}{\partial\mu_3}|_{\mu_B}. \tag{III.55}$$

We can then write $V^{(i,k)}_{WS} = V^{(i)}_{WS}$, $\rho^{(k)}_g = \rho_g$, $y^{(k)}_g = y_g$, and:

$$G^{1b}_{tot}(k) = -TV \ln z^{el}_\beta + \sum_i n^{(k)}_i \left(G^e_{\beta\mu_B\mu_3}(A^{(i)}_e, I^{(i)}_e) - TV^{(i,k)}_{WS} \ln z^{HM}_{\beta\mu_B\mu_3} \right), \tag{III.56}$$

where we have defined the in-medium modified cluster Gibbs energy:

$$G^e_{\beta\mu_B\mu_3}(A, \delta, \rho_g, y_g, \rho_p) = F^e_\beta - \mu_B A_e - \mu_3 I_e. \tag{III.57}$$

The thermodynamic limit implies that all the realizations correspond to the same (infinite) volume:

$$V = \sum_i n^{(k)}_i V^{(i,k)}_{WS}, \tag{III.58}$$

meaning that the gas contribution becomes completely independent of the cluster contribution, and fully determined by the chemical potentials

$$G^{1b}_{tot}(k) = -TV \ln \left(z^{el}_\beta z^{HM}_{\beta\mu_B\mu_3} \right) + \sum_i n^{(k)}_i G^e_{\beta\mu_B\mu_3}(A^{(i)}_e, I^{(i)}_e), \tag{III.59}$$

We are ready to calculate the one-body equivalent grandcanonical partition sum

$$Z^{1b} = \sum_k \exp -\beta G^{1b}_{tot}(k) = \left(z^{el}_\beta z^{HM}_{\beta\mu_B\mu_3} \right)^V Z^{cl}_{\beta\mu_B\mu_3}, \tag{III.60}$$

with

$$Z^{cl}_{\beta\mu_B\mu_3} = \sum_k \exp -\beta \sum_i n^{(k)}_i G^e_{\beta\mu_B\mu_3}(i) \tag{III.61}$$

$$= \prod_i \sum_{n=0}^{\infty} \frac{\left(\exp -\beta G^e_{\beta\mu_B\mu_3}(i) \right)^n}{n!} \tag{III.62}$$

$$= \prod_i \exp \omega_{\beta\mu_B\mu_3}(i). \tag{III.63}$$

With eq.(III.63) have recovered a NSE-like expression for the cluster multiplicities

$$< n_i >_{\beta,\mu,\mu_3} = \omega_{\beta\mu_B\mu_3}(i) \tag{III.64}$$

$$= \exp -\beta \left(F^e_\beta(A, \delta, \rho_g, y_g, \rho_p) - \mu_B A_e - \mu_3 I_e \right), \tag{III.65}$$

where the electron energy density and entropy density are known.

It is interesting to notice that the baryonic component (clusters as well as gas) only depend on the baryonic part of the total chemical potentials μ_B, μ_3. These chemical potentials are not the thermodynamic potentials conjugate to the densities μ'_B, μ'_3 which determine the thermodynamics; indeed they are shifted of the electron contribution. This explains why the phase transition is quenched in stellar matter even if the baryonic chemical potential μ_B has a backbending behavior as a function of the baryonic density [77]. This point will be further discussed in section III E.

From a practical point of view, the numerical implementation of the NSE model is simpler than the one if its approximation, namely the SNA. Indeed the variational character of the approach is fully exhausted by the construction of the partition sum, and no extra derivation of the energy functional has to be performed. This means that we can easily use fully realistic functionals for the cluster free-energies which are not analytically differentiable. Contrary to section III A, we therefore use the tables of experimental masses of Audi *et al.* [61] and, in order to extend the pool of nuclei for which pairing and shell effects are accounted for, evaluated masses of Duflo-Zuker [82] for the vacuum energies, the full list of low-lying resonances for light nuclei for the degeneracy factor g_β, and realistic level densities fitted from experimental data from ref.[81] in eq.(III.5). Only when this information is not available (or to make the quantitative comparisons with SNA as in section III D), we switch to the Skyrme-LDM mass model. Moreover, we explicitly consider isospin inhomogeneities in the spatial distribution of clusters due to Coulomb and skin effects. This is done considering that the bulk asymmetry δ entering in the in-medium correction to the cluster energies does not coincide with the global asymmetry $I = 1 - 2Z/A$. The bulk asymmetries δ, δ_e are linked to the global asymmetry $I_e = 1 - 2Z_e/A_e$ via gas density and composition as is given in Refs.[88–90]:

$$\delta = \left(1 - \frac{\rho_g}{\rho_0(\delta)}\right)\delta_e + \frac{\rho_g}{\rho_0(\delta)}\delta_g, \tag{III.66}$$

$$\delta_e = \frac{I_e + \frac{3a_C}{8Q}\frac{Z_e^2}{A_e^{5/3}}}{1 + \frac{9J_{sym}}{4Q}\frac{1}{A_e^{1/3}}}, \tag{III.67}$$

where $\delta_g = (\rho_{gn} - \rho_{gp})/\rho_g$, $J_{sym} = \epsilon_{sym}/\rho_0(0)$ is the symmetry energy per baryon at saturation, Q is the surface stiffness coefficient extracted from a semi-infinite nuclear matter calculation, and a_C is the Coulomb parameter taken equal to $a_C = 0.69$ MeV. This equation is consistently solved with the one giving the isospin dependence of the saturation density [54]

$$\rho_0(\delta) = \rho_0(0)\left(1 - \frac{3L_{sym}\delta^2}{K_{sat} + K_{sym}\delta^2}\right). \tag{III.68}$$

In expression (III.68), $K_{sat} = 9\rho_0^2\partial^2(\epsilon_{HM}/\rho)/\partial\rho^2|_{\rho_0}$ is the nuclear (symmetric) matter incompressibility, $L_{sym} = 3\rho_0\partial(\epsilon_{sym}/\rho)/\partial\rho|_{\rho_0}$ and $K_{sym} = 9\rho_0^2\partial^2(\epsilon_{sym}/\rho)/\partial\rho^2|_{\rho_0}$ are the slope and curvature of the symmetry energy at (symmetric) saturation, where we have introduced the usual definition of the symmetry energy density

$$\epsilon_{sym} = \frac{1}{2}\left.\frac{\partial^2\epsilon_{HM}}{\partial\delta^2}\right|_{\delta=0}. \tag{III.69}$$

It was shown in ref. [54, 60] that accounting for the difference between bulk and global asymmetry is a crucial point to obtain, within a cluster model, energy functionals compatible with microscopic calculations. Again, the difference between δ and I is neglected in the numerical applications of section III D, in order to compare the NSE and SNA approaches within the same definitions for the physical ingredients.

Our final result, eqs.(III.54),(III.55),(III.65) is formally very close to the different existing versions of grandcanonical extended NSE[41–43, 45, 46, 48, 49]. This is not surprising, since these equations simply state that all the different baryonic species are quasi-ideal gases of independent particles. However, some specificity of the proposed approach should be stressed.

It is clear from the microscopic modelizations of the Wigner Seitz cell at zero temperature that any realistic finite temperature model has to include in some way interactions between the clusters. The way of implementing these in medium effects is not unique, and the different treatments lead to a considerable spread in the predictions of extended NSE models[55].

The viewpoint we have taken in this paper is that the very definition of a Wigner-Seitz cell implies that WS cells are the correct variables that can be treated as independent degrees of freedom. This fully fixes the in-medium effect under the unique hypothesis that each cell contains only one bound cluster. As we have discussed in the introduction, this hypothesis, which is employed by all the existing models in the literature, is certainly not completely correct in general and some cluster-cluster interaction should be taken into account[59] to improve the present description.

The result of building a model on independent WS cells is that a NSE-like expression can be recovered for the cluster abundances, but with some specific features which insure that the zero temperature limit is properly obtained. Specifically, we can see from eq.(III.65) that the variable conjugated to the chemical potentials is not the physical cluster size (A, Z) but the reduced value (A_e, Z_e) (eqs.(II.6),(II.7)) which represents its bound part. Moreover, the cluster free energy has to be modified according to eq.(III.6) if one wants that in-medium effects are limited to a modification of the surface tension.

D. NSE versus SNA

To compare in greater detail the SNA to the NSE results, we can evaluate the most probable cluster mass and isospin A^{eq}, I^{eq} predicted by the NSE. This is obtained by maximizing the argument of the exponential in eq.(III.64):

$$dG^e = d\left(F^e_\beta - \mu_B A_e - \mu_3 I_e\right) = 0. \tag{III.70}$$

Since ρ_g, y_g are fixed, we can equivalently put to zero the partial derivatives with respect to A_e, I_e, or with respect to A, δ. The first choice leads to:

$$\mu_3 = \frac{\partial F^e_\beta}{\partial I_e}\left(A_e, I_e, \rho_g, y_g\right)|_{A_e,\rho_g,y_g}; \tag{III.71}$$

$$\mu_B = \frac{\partial F^e_\beta}{\partial A_e}\left(A_e, I_e, \rho_g, y_g\right)|_{I_e,\rho_g,y_g}. \tag{III.72}$$

These equations look very different from the equilibrium equations (III.8),(III.9) corresponding to the SNA. However they are far from being in a closed form. Indeed, the dependence on A_e, I_e of G^e is highly non trivial:

$$F^e_\beta(A, \delta) = F^e_\beta(A(A_e, \delta(A_e, I_e)), \delta(A_e, I_e)), \tag{III.73}$$

where the dependence of δ on A_e, I_e is obtained from the solution of the two coupled equations

$$\frac{I_e}{A_e} = \frac{\rho_0(\delta)}{\rho_0(\delta) - \rho_g}\left(\delta - \frac{y_g}{\rho_0(\delta)}\right); \tag{III.74}$$

$$A_e = A\frac{\rho_0(\delta) - \rho_g}{\rho_0(\delta)}. \tag{III.75}$$

This coupling will induce an effective coupling between the isoscalar and isovector chemical potential. After some algebra we get:

$$\frac{\partial E^e}{\partial A}|_\delta = \mu_B\frac{\rho_0 - \rho_g}{\rho_0} + \mu_3\frac{\rho_0\delta - y_g}{\rho_0} + \frac{3T}{2A} + T\frac{\partial \ln c_\beta}{\partial A}|_{\delta,\rho_g,y_g}; \tag{III.76}$$

$$\frac{\partial E^e}{\partial \delta}|_A = \mu_3 A\left(1 + \frac{y_g\rho_0'}{\rho_0^2}\right) + \mu_B A\frac{\rho_g\rho_0'}{\rho_0^2} + \frac{3}{2}T\frac{\rho_g}{\rho_0}\frac{\rho_0'}{\rho_0 - \rho_g} + T\frac{\partial \ln c_\beta}{\partial \delta}|_{A,\rho_g,y_g}. \tag{III.77}$$

These equations are similar, but not identical to the SNA equations (III.8),(III.9). The difference arises from the fact that the Wigner-Seitz volume as a variational variable in the SNA approach induces a complex coupling between the different equations. In the NSE, the Wigner-Seitz volume is trivially defined by the condition

$$V^{eq}_{WS} = \frac{Z^{eq}_e}{\rho_p - \rho_{pg}}. \tag{III.78}$$

Conversely, we have seen that the same result as in this grandcanonical approach is obtained if we consider a canonical problem with a large number of Wigner-Seitz cells. This is not surprising, because the neighboring cells act as a particle bath.

This result implies that we do not necessarily expect that the most probable cluster obtained in the complete NSE model exactly coincides with the result of the SNA approximation. This effect however turns out to be very small. A much more important source of difference between SNA and NSE is expected when the NSE distribution has multiple peaks of comparable height. In that case the (ρ_B, y_p) of the total distribution for a given set of chemical potentials is not the same as the one of the most probable cluster. This induces a non negligible shift between SNA and NSE even at very low temperatures.

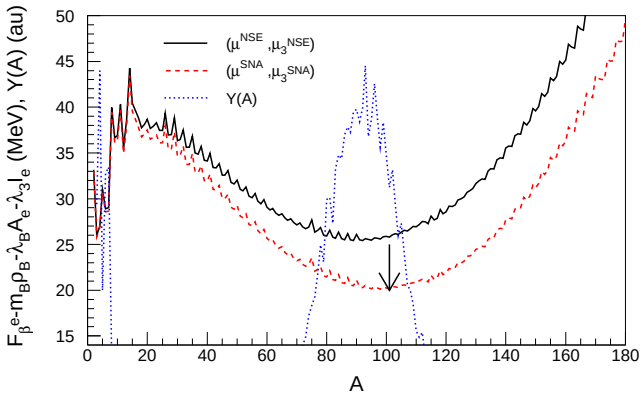

FIG. III.3: (Color online). Constrained cluster free energy for $\rho_B = 10^{-3}$ fm^{-3}, $T = 1.5$ MeV in β-equilibrium with chemical potentials corresponding to the NSE (full line) and SNA (dashed line) model, for a fixed cluster proton fraction corresponding to the minimum of the constrained free energy. The arrow gives the SNA solution. The dotted line gives the NSE multiplicity distribution in arbitrary units.

This point is explained in Fig.III.3 which shows the in-medium modified cluster free energy eq.(III.6) as a function of the cluster size. The free energy has been constrained with two Lagrange multipliers, corresponding to the chemical potentials obtained in the SNA and NSE model at an arbitrarily chosen thermodynamic point belonging to the β-equilibrium trajectory, $\rho_B = 10^{-3}$ fm^{-3} $T = 1.5$ MeV, $Y_p = 0.08503$. To allow a one-dimensional representation, a cut has been done with a plane whose $(1 - 2 \cdot Z^{eq}/A^{eq})$-value is as close as possible to the corresponding value of the constrained free energy minimum. The observed staggering stems from discrete values of $(1 - 2 \cdot Z^{eq}/A^{eq})$ and, for $A \leq 16$, structure effects accounted for in the experimental binding energy. The NSE abundancies are also represented in arbitrary units. We can see that the NSE abundancies correctly follow the shape of the constrained free energy, as implied by eq.(III.65). This means that for identical values of the chemical potentials in the two models, the optimal SNA cluster (indicated by an arrow in the example shown in the figure) should exactly coincide with the most probable NSE cluster. However, allowing clusters of any arbitrary size and composition obviously alters the mapping between density and chemical potential. The deviation of chemical potentials is typically very small (for the example shown in the figure, we have $\mu_B = -12.929(-12.889)$ MeV , $\mu_3 = 13.547(13.507)$ MeV for NSE (SNA)), but it is sufficient to modify the position of the constrained energy minimum. As a consequence, a SNA treatment cannot correctly identify the most probable cluster.

NSE predictions were already compared to the SNA approximation, both at fixed proton fraction and in β-equilibrium, in Fig.III.1 above. We can see that, except the very low densities where light cluster degrees of freedom are important, at low temperature the NSE model is very close to SNA. However the consideration of clusters of all sizes naturally leads to a reduction of the cluster size at high density and high temperature, similar to the LS equation of state because of the particular treatment of α particles in that model. It is however important to notice that in the complete NSE α particles are only abundant for matter close to isospin symmetry, while more neutron rich hydrogen and helium isotopes prevail in neutron rich matter. This aspect, which by construction cannot be addressed in the LS model, will be discussed in greater detail later.

At higher temperature the NSE distribution is spread over a large domain of cluster sizes and isospin (see the right panel of Fig. III.2), and the deviation both with SNA and with the LS equation of state becomes very large. In particular, the abundances are dominated by light resonances and the heavy cluster yield becomes increasingly negligible with increasing temperature.

A more detailed comparison between SNA and NSE is given by Fig.III.4 in terms of the unique/most probable cluster mass (left panels) and relative mass fraction of unbound nucleons (right panels). For NSE, the most abundant cluster mass is plotted against the average mass of heavy clusters arbitrarily defined as clusters with $A \geq 20$.

As in the previous figure the left panels show that, whatever the density, increasing temperature leads to an increased deviation between the average SNA composition and the most probable NSE cluster. A huge part of this difference can be explained by the importance of accounting for (a variety of) light clusters which are entropically favored at increasing temperature. This is confirmed by the lower part of the figure, where the thin lines have been obtained by artificially switching to zero the statistical weight of all clusters lighter than $A = 20$. We can see that neglecting light clusters considerably approaches SNA to NSE, even if residual differences still persist partially because of the shift in

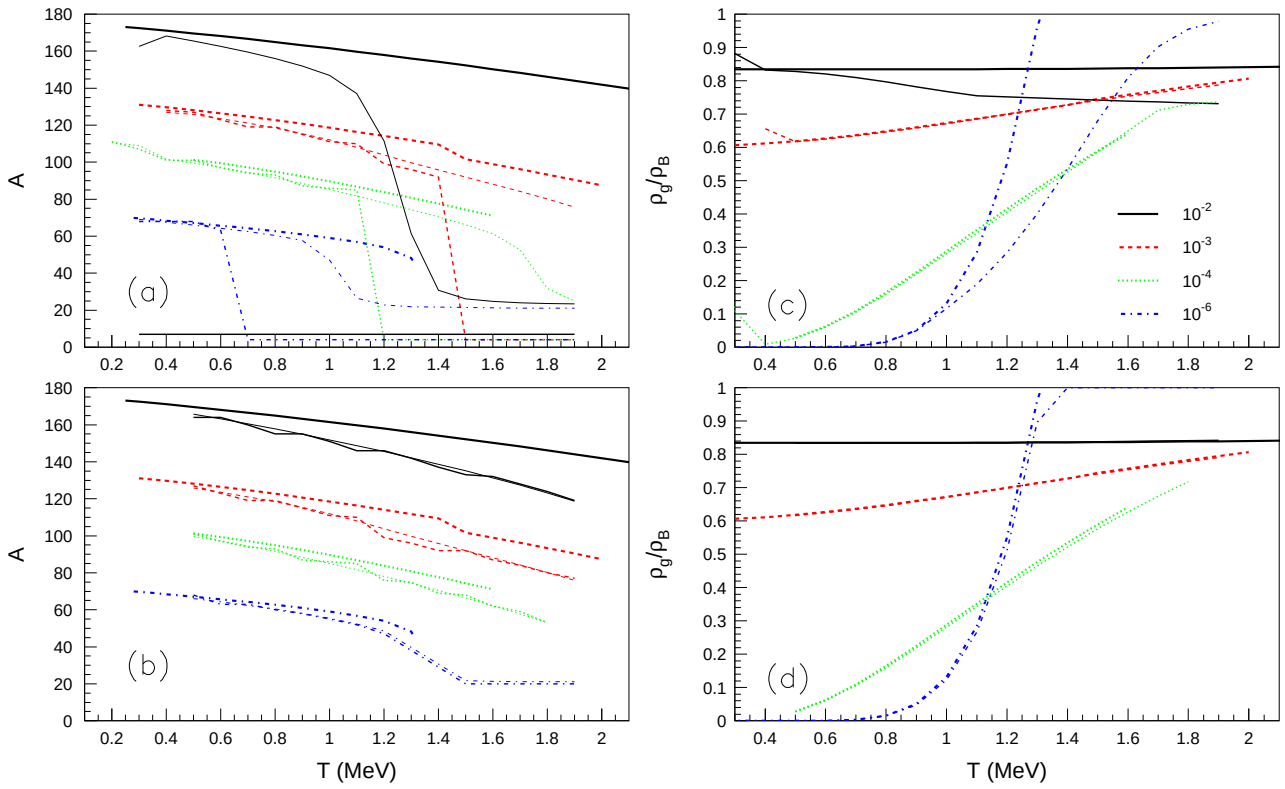

FIG. III.4: (Color online). Structure of the (P)NS crust at $\beta-$equilibrium as a function of temperature for different values of the baryonic density $\rho_B = 10^{-6}, 10^{-4}, 10^{-3}, 10^{-2}$ fm^{-3}; Thick and middle thick lines correspond to predictions of SNA and, respectively, most abundant cluster in NSE. Thin lines correspond to the average heavy ($A \geq 20$) cluster atomic mass in NSE. Bottom: the standard NSE is here replaced with a version in which no cluster lighter than $A = 20$ is allowed to exist. Left: average cluster size. Right: relative amount of unbound nucleons. In SNA Skyrme-LDM [62] binding energies have been used. In NSE, experimental data [61] have been used for the binding energies of nuclides with $A < 16$ and Skyrme-LDM [62] predictions otherwise. The considered effective interaction is SLY4.

chemical potentials discussed above. A complementary view is offered by the right panels. At intermediate densities ($\rho_B = 10^{-4}, 10^{-3}$ fm^{-3}) and $T > 0.5$ MeV, SNA and NSE predictions agree in the percentage of unbound nucleons, thus indicating that the chemical potentials of the two models have close values (recall that at a given temperature the gas density only depends on the chemical potential).

At variance with this, the extreme densities show a strong reduction of the nucleon gas in NSE with increasing temperature. At the lowest density displayed $\rho_B = 10^{-6}$ fm^{-3} where matter as a whole is close to isospin symmetry, this comes from the enhanced production of ^{2}H and ^{4}He at the cost of unbound nucleons. At the highest density $\rho_B = 10^{-2}$ fm^{-3} the opposite holds. The extreme neutron enrichment of β-equilibrated matter favors copious production of isospin asymmetric hydrogen and helium isotopes leaving thus less unbound nucleons. The suppresion of clusters with $A < 20$ (right bottom panel) confirms the above reasoning by showing a perfect agreement between SNA and NSE everywhere except $\rho_B = 10^{-6}$ fm^{-3} and $T \geq 1.5$ MeV where $\rho_{cl}/\rho_B \to 0$.

The global behavior of the β-equilibrated matter composition in the NSE model is shown in Figs. III.5, III.6. In Fig. III.5 average mass, charge and mass fraction of heavy ($A \geq 20$) nuclei are plotted as a function of density for temperatures ranging from 0.4 to 2 MeV. Fig. III.6 presents, for the same temperatures, the mass fractions of unbound neutrons and protons together with the mass fraction of different light species (^{2}H, ^{3}H, ^{4}He, $^{A\geq4}$H, $^{A\geq5}$He) as a function of density. As mentioned in the figure captions, in these cases experimental values [61] and DZ10 [82] predictions have been used for nuclear masses. The unbound nucleon component is treated according to SLY4.

We can again observe the nice convergence towards the zero temperature composition of the Wigner-Seitz cell, as well as the complex behavior as a function of density for all temperatures, leading to a melting of the clusters in the nuclear medium at a density of the order of $\rho_B = 0.01$ fm^{-3}. As it is well known in the literature, the exact value of the transition density depends on the effective interaction. We do not try to make such a study here because the

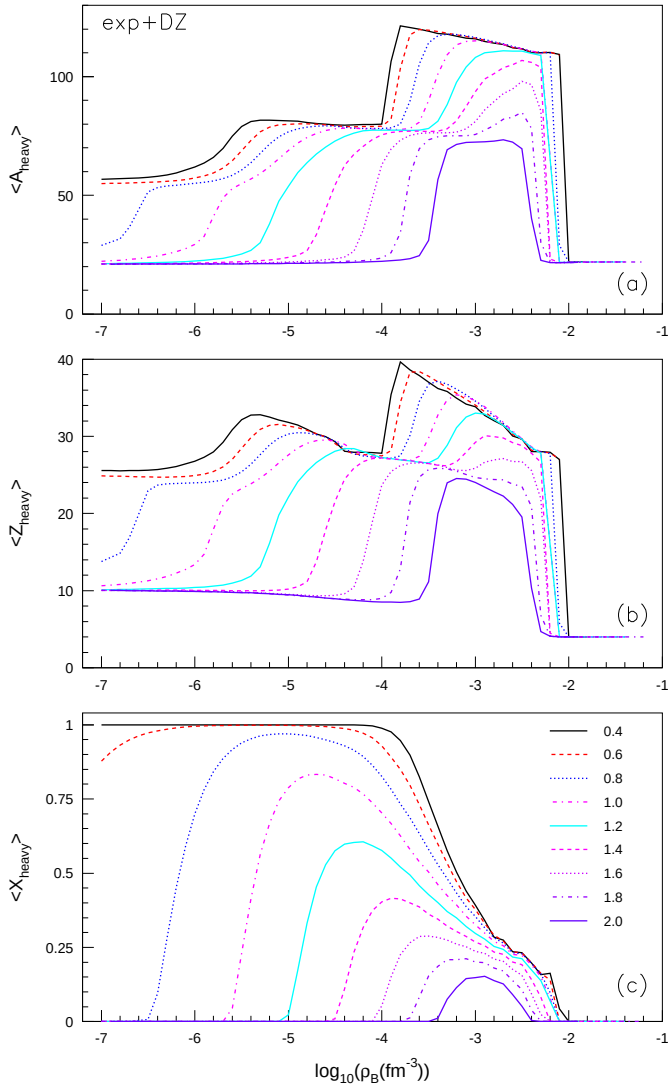

FIG. III.5: (Color online). NSE results at $\beta-$equilibrium for different densities and temperatures (expressed in MeV and listed in the key legend). Upper and middle panels: average mass and atomic numbers of clusters heavier than $A = 20$. Lower panel: corresponding mass fraction. Experimental and DZ10 [82] nuclear masses have been considered for clusters. The SLY4 effective interaction was used for the unbound nucleon component.

presence of deformation degrees of freedom in the form of pasta phases, here neglected, would most probably modify the value of the transition density. Inspection of Fig. III.6 reveals the importance of accounting for all the different light nuclear species and not limiting to deuteron and α-particles. This is true for any proton fraction, but particularly clear in the very neutron rich matter implied by β-equilibrium, where light unbound resonances completely dominate, together with unbound neutrons, the matter composition at high temperature.

E. Thermodynamics and electrons

The problem of the grandcanonical formulation which has been recently observed[71, 77] is that baryonic matter at sub-saturation densities presents a first order liquid-gas phase transition which is signaled by the fact that a huge part of the phase diagram is jumped over if one imposes constant chemical potentials[47, 77].

As we have discussed in section II E, this instability is not physical and only comes from the fact that the electron contribution is neglected in the instability analysis. If the electron free energy is accounted for, the dependence of the

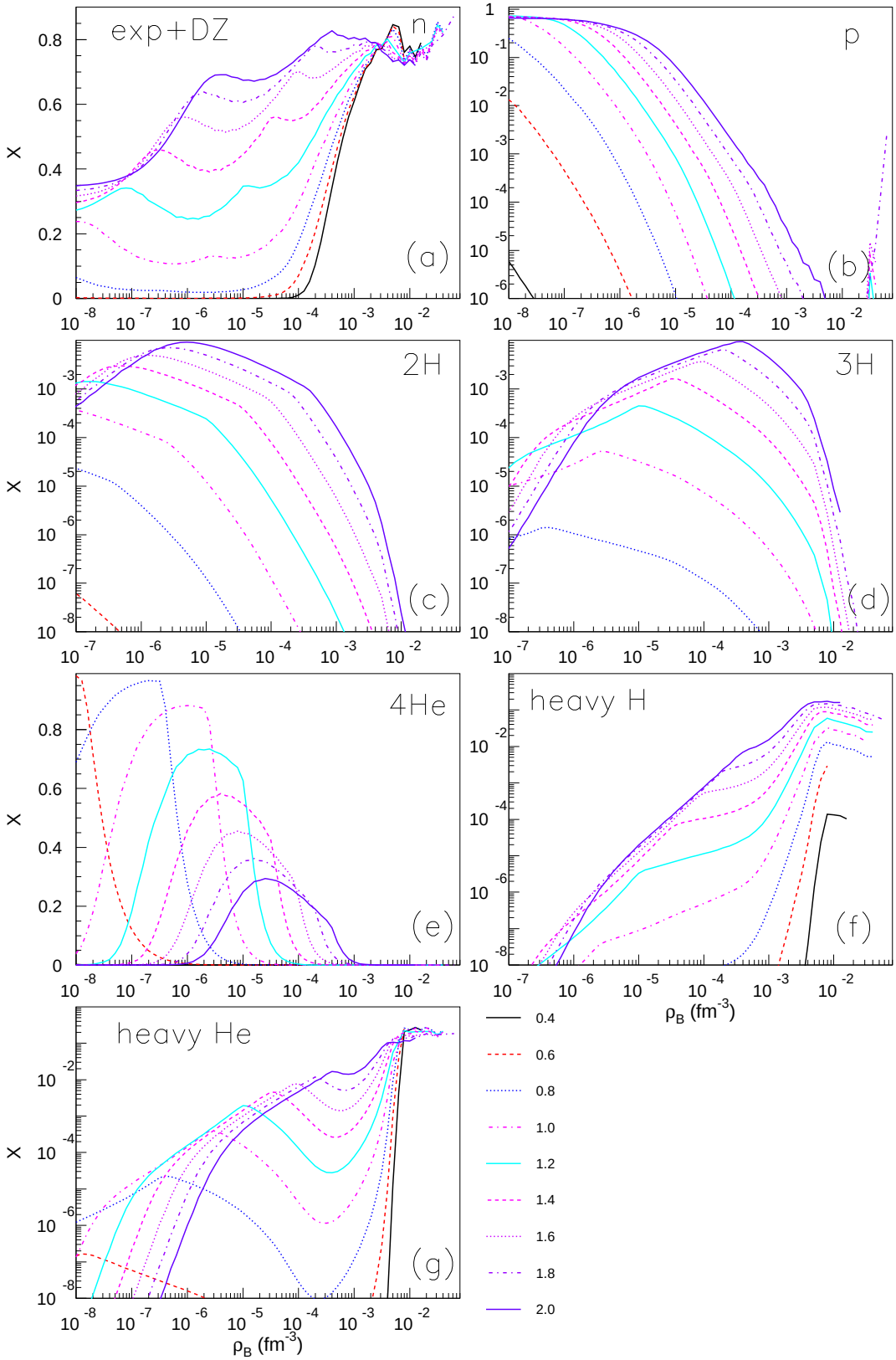

FIG. III.6: (Color online). NSE mass fractions of unbound nucleons and 2H, 3H, 3He, 4He, $^{4\leq A}$H and $^{5\leq A}$He at $\beta-$equilibrium for different densities and temperatures expressed in MeV and listed in the key legend. Experimental [61] and DZ10 [82] data have been used for the binding energies. The SLY4 effective interaction was used for the unbound nucleon component. Note that X-axis range is not the same in all panels.

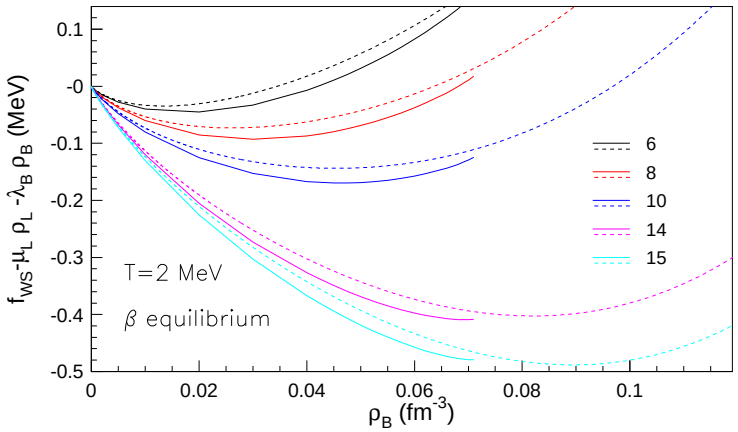

FIG. III.7: (Color online). Behavior of the constrained free energy in β-equilibrium ($\mu_L = 0$) for the clusterized phase (full line) and the homogeneous phase (dashed line) at different values of the baryonic chemical potential λ_B mentioned in the key legend (in MeV). Experimental binding energies and predictions of the 10-parameter mass model of Duflo-Zuker are used for the nuclear clusters. For the unbound nucleon gas the SLY4 effective interaction has been used.

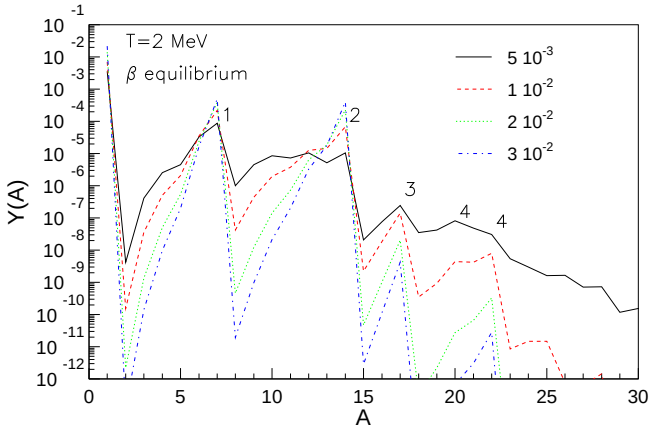

FIG. III.8: (Color online). Fragment mass distributions corresponding to β-equilibrium, T=2 MeV and different baryonic densities (expressed in fm^{-3}) as listed in the key legend. The numbers next to peaks specify the charge number of the most abundant nucleus.

free energy density on the baryonic density reads

$$f(\rho_B, \rho_p) = f_B(\rho_B, \rho_p) + f_{el}(\rho_p), \tag{III.79}$$

where f_B denotes the baryonic part and the Coulomb interaction part between protons and electrons. The relations (II.38) between density and chemical potential are shifted because of the electron contribution

$$\mu_B \to \mu'_B = \mu_B + \frac{1}{2}\mu_{el} \;\; ; \;\; \mu_3 \to \mu'_I = \mu_3 - \frac{1}{2}\mu_{el}, \tag{III.80}$$

and the curvature of the constrained free energy density is augmented of a positive term as:

$$\frac{\partial^2 f}{\partial \rho_B^2} = \frac{\partial \mu_B}{\partial \rho_B} + \frac{1}{2}\frac{\partial \mu_e}{\partial \rho_e}. \tag{III.81}$$

This quenching of the phase transition has as a practical consequence that a one-to-one correspondence between density and chemical potential exists in stellar matter, meaning that it is possible to describe all the possible density configurations in a grandcanonical treatment, provided the electron contribution is accounted for. In that case, the

ensemble equivalence is recovered and the associated partitions are by construction identical to the ones obtained in a canonical model, as we have explicitly demonstrated in sections III B,III C.

It is however in principle perfectly possible that a residual convexity persists in the constrained free energy (III.81). In that case, a first order phase transition reminiscent of liquid-gas would survive in stellar matter. Such a phenomenology was recently suggested in ref.[71] and evidenced, for T=0, in the right panel of Fig.II.4.

To answer to this question, we show in Fig.III.7 the comparison between the constrained free energy energy density of the clusterized Wigner-Seitz cell, and the one corresponding to homogeneous matter, for different values of the baryonic chemical potential (mentioned in the key legend), at a representative temperature of 2 MeV. We can see that the clusterized phase systematically presents a lower free energy density than the homogeneous system, for all chemical potentials up to about $\mu_B = 14$ MeV. For the highest considered chemical potential, 15 MeV, the constrained energy minimum corresponds to homogeneous matter. This means that the first order phase transition is restricted to a density domain between about $\rho_B = 0.07$ and $\rho_B = 0.09$ fm^{-3}. These values obviously depend on the temperature and on the effective interaction, but still the associated density discontinuity is too small to have any observable effects. Moreover, we have to stress again that we have disregarded deformation degrees of freedom in this model. The inclusion of highly deformed pasta clusters would lead to a lowering of the clusterized phase, and an extra shrinking of the possible transition domain.

Figure III.8 shows the detailed matter composition in the high density region close to the transition to homogeneous matter. Dominance of exotic light nuclei as ^{7}H, ^{14}He, ^{17}Li, ^{20}Be, ^{22}Be is worthwhile to note meaning that it is very important to account for light clusters in that domain. It is therefore possible that smoother transitions would be observed between the different pasta phases, and between the pasta phase and homogeneous matter, if light clusters were accounted for. We leave this point to future developments.

IV. CONCLUSIONS

In this paper we have presented a unified treatment of the stellar matter composition and equation of state in the sub-saturation regime, which can be applied at any temperature, density and proton fraction.

The basic idea of the model is to consider stellar matter as a statistical mixing of independent Wigner-Seitz cells. The individual composition in terms of bound and unbound particles does not minimize the free energy density, but the combination of different cells does.

The result is a set of NSE-like equations for the cluster abundancies, where both the bulk and the surface part of the cluster self-energies are modified by the presence of free nucleon scattering states, and a high energy cut naturally appears in the cluster internal state partition sum. The model dependence of the finite temperature model is thus limited to the model dependence of the treatment of the Wigner-Seitz cell, which in turn is very well constrained by microscopic calculations, with a residual uncertainty limited to the density dependence of the symmetry energy in the underlying effective interaction. In the present applications, the in-medium modifications are treated in the local density approximation, but it will be extremely interesting to map them from a more sophisticated microscopic, and possibly beyond mean-field treatment in the next future.

We have analytically shown that, for a given set of chemical potentials, the most probable cell composition coincides with the one which is obtained by the standard variational procedure assuming one single representative cluster. This guarantees that the model has the correct zero temperature limit.

However, the simultaneous presence of many different clusters in each thermodynamic condition modifies the relation between density and chemical potential with respect to the single nucleus approximation. As a consequence, stellar matter predictions of this improved NSE model differ from the SNA approximation even at the level of the most probable composition, and even at temperatures lower than 1 MeV.

We have specifically shown quantitative applications in β-equilibrium. The dominant configuration is a mixture of clusters of different mass and atomic numbers. This effect is due at low density to the non-monotonic behavior of the cluster energies due to shell and sub-shell closures, and at high density to the flatness or multi-minima of the free-energy landscape for very neutron rich matter. None of these features can be accounted in a SNA approach. In addition to the multi-peaked cluster distribution we have seen that very light clusters appear with a probability compared to the one of heavier clusters. This feature is accounted in the Lattimer-Swesty SNA model by including α-particles in the single representative Wigner-Seitz cell. We can see that this is physically correct at the lowest densities, which at β-equilibrium correspond to matter close to isospin symmetry. Conversely, in very asymmetric matter as it can be found at β-equilibrium at higher density, the most probable light cluster is never a α particle, but rather the last bound isotope of H and He. It is therefore clear that at finite temperature other light particles than α have to be included in the equilibrium.

Acknowledgments

Discussions with Stefan Typel are gratefully acknowledged. This work has been partially funded by the SN2NS project ANR-10-BLAN-0503 and it has been supported by NewCompstar, COST Action MP1304. Ad. R. R acknowledges partial support from the Romanian National Authority for Scientific Research under grants PN-II-ID-PCE-2011-3-0092 and PN 09 37 01 05 and kind hospitality from LPC-Caen.

[1] G. Baym, C. Pethick, P. Sutherland, Astroph. J **170**, 299 (1971).
[2] G. Baym, H. A. Bethe and C.Pethick, Nucl. Phys. **A175**, 225 (1971).
[3] D. G. Ravenhall, C.J. Pethick, J.R. Wilson, Phys. Rev. Lett. **50**, 2066 (1983).
[4] M. Hashimoto, H. Seki, M. Yamada, Prog. Theor. Phys. **71**, 320 (1984).
[5] J. M. Lattimer, C. J. Pethick, D. G. Ravenhall, D. Q. Lamb, Nucl. Phys. **A432**, 646 (1985).
[6] G. Watanabe, K. Iida, K. Sato, Nucl. Phys. **A676**, 455 (2000).
[7] F. Douchin, P. Haensel, Phys. Lett. **B 485**, 107 (2000).
[8] J. W. Negele and D. Vautherin, Nucl. Phys. **A207**, 298 (1973).
[9] E. Chabanat, P. Bonche, P. Haensel, J. Meyer, R. Schaeffer, Nucl. Phys. **A635**, 231 (1998).
[10] S. Goriely, N. Chamel, and J. M. Pearson, Phys. Rev. **C 88**, 061302(R) (2013).
[11] M. Dutra et al., Phys. Rev. **C 85**, 035201 (2012).
[12] M. Dutra et al., Phys. Rev. **C 90**, 055203 (2014).
[13] F. Douchin, P. Haensel, Astron. Astrophys. 380, 151 (2001).
[14] T. Maruyama, T. Tatsumi, D. N. Voskresensky *et al.*, Phys. Rev. **C 72**, 015802 (2005).
[15] M. Baldo, U. Lombardo, E. E. Saperstein *et al.*, Nucl. Phys. **A750**, 409 (2005).
[16] J. M. Pearson, N. Chamel, S. Goriely, *et al.*, Phys. Rev. **C 85**, 065803 (2012).
[17] A. Pastore, J. Margueron, P. Schuck *et al.*, Phys. Rev. **C 88**, 034314 (2013).
[18] F. Grill, H. Pais, C. Providencia *et al.*, Phys. Rev **C 90**, 045803 (2014).
[19] H. Pais and J. R. Stone, Phys. Rev. Lett. **109**, 151101 (2012).
[20] Topical Issue on Nuclear Symmetry Energy, B. A. Li, A. Ramos, G. Verde, I. Vidana editors, Eur. Phys. J. **A 50** (2014).
[21] A. Roggero, A. Mukherjee, F. Pederiva, Phys. Rev. Lett. **112**, 221103 (2014).
[22] W. Zuo, I. Bombaci, U. Lombardo, Eur. Phys. J. **A 50**, 12 (2014).
[23] C. Drischler, V. Soma, A. Schwenk, Phys. Rev. **C 89**, 025806 (2014).
[24] F. Sammarruca, B. Chen, L. Coraggio, *et al.* Phys. Rev. **C 86**, 054317 (2012).
[25] K. Sumiyoshi, H. Kuwabara, H. Toki, Nucl. Phys. **A 581**, 725 (1995).
[26] S. S. Avancini, D. P. Menezes, M. D. Alloy *et al.*, Phys. Rev. **C 78**, 015802 (2008).
[27] N. Sandulescu, Phys. Rev. **C 70**, 025801 (2004).
[28] M. Fortin, F. Grill, J. Margueron, D. Page, and N. Sandulescu, Phys. Rev. **C 82**, 065804 (2010).
[29] M. Onsi, A. K. Dutta, H. Chatri, *et al.* Phys. Rev. **C 77**, 065805 (2008).
[30] S. S. Avancini, S. Chiacchiera, D. P. Menezes, *et al.* Phys. Rev. **C 82**, 055807 (2010).
[31] W. G. Newton, J. R. Stone, Phys. Rev. **C 79**, 055801 (2009).
[32] B. Schuetrumpf, M. A. Klatt, K. Iida, *et al.*, Phys. Rev. **C 87**, 055805 (2013).
[33] J.M. Lattimer, C.J. Pethick, D.G. Ravenhall, D.Q. Lamb, Nucl. Phys. **A 432**, 646 (1985).
[34] F. Sebille, S. Figerou, and V. de la Mota, Nucl. Phys. **A 822**, 51 (2009).
[35] J. M. Lattimer and F. D. Swesty, Nucl. Phys. **A535**, 331 (1991).
[36] H. Shen, H. Toki, K. Oyamatsu, and K. Sumiyoshi, Nucl. Phys. **A 637**, 435 (1998); H. Shen, H. Toki, K. Oyamatsu *et al.*, Astrophys. J. Suppl.Series **197**, 20 (2011).
[37] A. Burrows and J. Lattimer, Astron. J. **285**, 294 (1984).
[38] M. B. Aufderheide, I. Fushiki, S. E. Woosley, D. A. Hartmann, Astrophys. J. Suppl.Series **91**, 389 (1994).
[39] A. Juodagalvis, K. Langanke, W. R. Hix, G. Martnez-Pinedo, J. M. Sampaio, Nucl. Phys. **A848**, 454 (2010).
[40] A. C. Phillips, The Physics of Stars, Manchester Physics Series (Wiley and Sons, Chichester, 1999).
[41] A. S. Botvina and I. N. Mishustin, Nucl. Phys. **A 843**, 98 (2010).
[42] S. R. Souza, B. V. Carlson, R. Donangelo, W. G. Lynch, A. W.Steiner and M. B. Tsang, Phys. Rev. **C 79**, 054602 (2009).
[43] S. I. Blinnikov, I. V. Panov, M. A. Rudzsky, and K. Sumiyoshi, Astron. Astrophys. **535**, A37 (2011).
[44] W. Hillebrandt, R. Wolf, and K. Nomoto, Astron. Astrophys. **133**, 175 (1984).
[45] S. Heckel, P. P. Schneider, A. Sedrakian, Phys. Rev. **C 80**, 015805 (2009).
[46] M. Hempel and J. Schaffner-Bielich, Nucl. Phys. **A 837**, 210 (2010); M. Hempel, T. Fischer, J. Schaffner-Bielich *et al.* Astrophys. J. **748**, 70 (2012).
[47] A. R. Raduta and F. Gulminelli, Phys. Rev. **C 82**, 065801 (2010).
[48] A. R. Raduta, F. Gulminelli and F. Aymard, Eur. Phys. J. **A 50**, 24 (2014).
[49] S. Furusawa, K. Sumiyoshi, S. Yamada, and H. Suzuki, Astrophys. J., **772**, 95 (2013).
[50] C. J. Horowitz, A. Schwenk, Nucl. Phys. **A 776**, 55 (2006).
[51] S. K. Samaddar, J. N. De, X. Vinas, and M. Centelles Phys. Rev. **C 80**, 035803 (2009).

[52] S. Typel, G. Roepke, T. Klhn, D. Blaschke, H. H. Wolter, Phys. Rev. C **81**, 015803 (2010).
[53] M. Hempel, J. Schaffner-Bielich, S. Typel, and G. Ropke, Phys. Rev. **C 84**, 055804 (2011).
[54] P. Papakonstantinou, J. Margueron, F. Gulminelli, Ad. R. Raduta, Phys. Rev. C **88**, 045805 (2013).
[55] N. Buyukcizmeci, A. S. Botvina, I. N. Mishustin, R. Ogul, M.Hempel, J. Schaffner-Bielich, F.-K. Thielemann, S. Furusawa, K. Sumiyoshi, S. Yamada, and H. Suzuki, Nucl. Phys. **A 907**, 13 (2013).
[56] K. Sumiyoshi, S. Yamada, H. Suzuki, *et al.*, Astrophys. J. **629**, 922 (2005).
[57] T. Fischer, M. Hempel, I. Sagert *et al.*, Eur. Phys. J. **A 50**, 46 (2014).
[58] S. S. Avancini, C. C. Barros Jr., L. Brito, S. Chiacchiera, D. P. Menezes, and C. Providencia, Phys. Rev. **C 85**, 035806 (2012).
[59] S. Typel, Phys. Rev. **C 89**, 064321 (2014).
[60] F. Aymard, F. Gulminelli and J. Margueron, Phys. Rev. C **89**, 065807 (2014).
[61] G.Audi, M. Wang, A. H. Wapstra, F. G. Kondev, M. MacCormick, X. Xu, and B. Pfeiffer, Chinese Physics **C36**, 1287 (2012); M. Wang, G. Audi, A. H. Wapstra, F. G. Kondev, M. MacCormick, X. Xu, and B. Pfeiffer, Chinese Physics **C36**, 1603 (2012); http://amdc.impcas.ac.cn/evaluation/data2012/data/nubase.mas12.
[62] P. Danielewicz and J. Lee, Nucl. Phys. **A818**, 36 (2009).
[63] F. Aymard, F. Gulminelli, and J. Margueron, in preparation.
[64] P. Haensel, J. L. Zdunik, and J. Dobaczewski, Astron. Astrophys. **222**, 353 (1989).
[65] P. Haensel and B. Pichon, Astron. Astrophys. **283**, 313 (1994).
[66] S. B. Ruster, M. Hempel, and J. Schaffner-Bielich, Phys. Rev. **C 73**, 035804 (2006).
[67] X. Roca-Maza and J. Piekarewicz, Phys. Rev. C **78** 025807 (2008).
[68] J. M. Pearson, N. Chamel, S. Goriely, and C. Ducoin, Phys.Rev.C **85**, 065803 (2012).
[69] P. Moller, J. R. Nix, W. D. Myers and W. J. Swiatecki, ADNDT **59**, 185 (1995).
[70] A. R. Raduta, F. Gulminelli, F. Aymard, EPJ **A 50**,24 (2014).
[71] H. Pais, W. G. Newton, and J. R. Stone Phys. Rev. **C 90**, 065802 (2014).
[72] C. J. Pethick, D. G. Ravenhall, C. P. Lorentz, Nucl. Phys. **A 584** 675 (1995) .
[73] C. Ducoin, Ph. Chomaz, and F. Gulminelli, Nucl. Phys. **A771**, 68 (2006).
[74] C. Providencia, L. Brito, S. S. Avancini, D. P. Menezes, Ph. Chomaz, Phys. Rev. **C 73** 025805 (2006).
[75] C. Ducoin, Ph. Chomaz, and F. Gulminelli, Nucl. Phys. **A789**, 403 (2007).
[76] P. Napolitani, P. Chomaz, F. Gulminelli, and K. H. O. Hasnaoui, Phys. Rev. Lett. **98**, 131102 (2007).
[77] F. Gulminelli and A. R. Raduta, Phys. Rev. **C 85**, 025803 (2012).
[78] C. J. Horowitz, M. A. Perez-Garcia, D. K. Berry, and J. Piekarewicz, Phys. Rev. **C 72**, 035801 (2005).
[79] H. Sonoda, G. Watanabe, K. Sato, K. Yasuoka, and T. Ebisuzaki, Phys. Rev. **C 77**, 035806 (2008); G. Watanabe, H. Sonoda, T. Maruyama, K. Sato, K. Yasuoka, and T. Ebisuzaki, Phys. Rev. Lett. 103, 121101 (2009).
[80] N. Glendenning, Phys. Lett. **B114**, 392 (1982).
[81] T. von Egidy and D. Bucurescu, Phys. Rev. C **72**, 044311 (2005); *ibid.*, Phys. Rev. C **73**, 049901(E) (2006).
[82] J. Duflo and A. P. Zuker, Phys. Rev. C **52**, R23 (1995).
[83] CompStar Online Supernovae Equations of State (CompOSE), http://compose.obspm.fr/, LS220.
[84] B. Carter, N. Chamel, and P. Haensel, Nucl. Phys. **A 748**, 675 (2005).
[85] F. Gulminelli, T. Furuta, O. Juillet, and C. Leclercq, Phys. Rev. **C 84**, 065806 (2011).
[86] C. B. Das, S. DasGupta, W. G. Lynch, A. Z. Mekjian, M. B. Tsang, Phys. Rep. **406**, 1 (2005).
[87] R. Balian, From Microphysics to Macrophysics, Springer Verlag, 1982.
[88] W. D. Myers and W. J. Swiatecki, Nucl. Phys. **A 336**, 267 (1980).
[89] M. Centelles, M. D. Estal, and X. Vinas, Nucl. Phys. **A 635**, 193 (1998).
[90] M. Warda, X. Vinas, X. Roca-Maza, and M. Centelles, Phys. Rev. **C 80**, 024316 (2009).